

Cosmic evolution of submillimeter galaxies and their contribution to stellar mass assembly

Michał J. Michałowski^{1,2}, Jens Hjorth¹, and Darach Watson¹

¹ Dark Cosmology Centre, Niels Bohr Institute, University of Copenhagen, Juliane Maries Vej 30, DK-2100 Copenhagen Ø, Denmark, michal@dark-cosmology.dk

² Scottish Universities Physics Alliance, Institute for Astronomy, University of Edinburgh, Royal Observatory, Edinburgh, EH9 3HJ, UK

Preprint online version: October 29, 2018

ABSTRACT

The nature of galaxies selected at submillimeter wavelengths (SMGs, $S_{850} \gtrsim 3$ mJy), some of the bolometrically most luminous objects at high redshifts, is still elusive. In particular their star formation histories and source of emission are not accurately constrained. In this paper we introduce a new approach to analyse the SMG data. Namely, we present the first self-consistent UV-to-radio spectral energy distribution fits of 76 SMGs with spectroscopic redshifts using all photometric datapoints from ultraviolet to radio simultaneously. We find that they are highly star-forming (median star formation rate $713 M_{\odot} \text{ yr}^{-1}$ for SMGs at $z > 0.5$), moderately dust-obscured (median $A_V \sim 2$ mag), hosting significant stellar populations (median stellar mass $3.7 \times 10^{11} M_{\odot}$) of which only a minor part has been formed in the ongoing starburst episode. This implies that in the past, SMGs experienced either another starburst episode or merger with several galaxies. The properties of SMGs suggest that they are progenitors of present-day elliptical galaxies. We find that these bright SMGs contribute significantly to the cosmic star formation rate density ($\sim 20\%$) and stellar mass density ($\sim 30\text{--}50\%$) at redshifts 2–4. Using number counts at low fluxes we find that as much as 80% of the cosmic star formation at these redshifts took place in SMGs brighter than 0.1 mJy. We find evidence that a linear infrared-radio correlation holds for SMGs in an unchanged form up to redshift of 3.6, though its normalization is offset from the local relation by a factor of ~ 2.1 towards higher radio luminosities. We present a compilation of photometry data of SMGs and determinations of cosmic SFR and stellar mass densities.

Key words. galaxies: active – galaxies: evolution – galaxies: high-redshift – galaxies: ISM – galaxies: starburst – submillimeter

1. Introduction

Submillimeter galaxies (SMGs; see Blain et al., 2002) were discovered at $850 \mu\text{m}$ ($S_{850} \gtrsim 3$ mJy) by the Submillimetre Common-User Bolometer Array (SCUBA; Holland et al., 1999) mounted on the James Clerk Maxwell Telescope (JCMT). Due to the coarse resolution of SCUBA, localizations derived from high-resolution radio maps had to be used to measure their spectroscopic redshifts (Chapman et al., 2005). Lots of studies have addressed the issue of characterizing the nature of SMGs (Egami et al., 2004; Greve et al., 2004, 2005; Smail et al., 2004; Swinbank et al., 2004, 2006, 2008; Takagi et al., 2004; Alexander et al., 2005; Borys et al., 2005; Kovács et al., 2006; Laurent et al., 2006; Pope et al., 2006; Tacconi et al., 2006, 2008; Takata et al., 2006; Younger et al., 2007, 2008, 2009a; Clements et al., 2008; Coppin et al., 2008; Dye et al., 2008, 2009; Hainline, 2008; Hainline et al., 2009; Perera et al., 2008; Scott et al., 2008; Austermann et al., 2009; Devlin et al., 2009; Eales et al., 2009; Murphy et al., 2009; Murphy, 2009; Tamura et al., 2009; Weiß et al., 2009b; Aravena et al., 2010, some of these works were based on surveys with sensitivity worse than 3 mJy quoted above). However they were usually based on limited samples ($\lesssim 20$ sources), limited wavelength coverage or photometric redshifts. These limitations have made it difficult

to solve several issues, including the characterization of the star formation histories of SMGs and their dominant source of emission.

An important open question concerns the contribution of SMGs to cosmic stellar mass assembly. This is important, because in order to understand galaxy evolution, the build-up of stellar mass must be mapped out to high redshifts. It is usually parametrized by the total star formation rate (SFR) density per unit comoving volume, (ρ_{SFR} ; see e.g. Hopkins, 2004; Hopkins & Beacom, 2006). At high redshifts it is difficult to disentangle the contribution to ρ_{SFR} from galaxy populations of different masses due to incompleteness at low luminosities.

Another approach to study stellar mass assembly is to consider directly the stellar mass density per unit comoving volume, ρ_* , which is equivalent to the integrated ρ_{SFR} over the age of the Universe. It is established that ρ_* grows with cosmic time (stellar mass is accumulating; Drory et al., 2005; Fontana et al., 2006; Elsner et al., 2008; Pérez-González et al., 2008; Marchesini et al., 2009), but the contribution from different galaxy populations is not well-determined. *Spitzer* observations of SMGs (Egami et al., 2004; Frayer et al., 2004; Ivison et al., 2004; Borys et al., 2005; Ashby et al., 2006; Laurent et al., 2006; Pope et al., 2006; Dye et al., 2008; Hainline, 2008; Hainline et al., 2009) have enabled studies of the rest-frame

near-infrared (near-IR) part of the spectrum, where old stellar populations are dominant – an important step forward in getting full spectral energy distributions and accurate estimates of stellar masses of SMGs. The results indicate that SMGs are among the most massive galaxies in the Universe.

The dominant source of emission from SMGs is dust reprocessed emission either from young stars or active galactic nuclei (AGNs). One way to test it is to compare the infrared (IR) and radio luminosities of SMGs, because, at least locally, star-forming galaxies follow a remarkably tight correlation between IR and radio luminosities (Helou et al., 1985; Condon, 1992). The correlation is believed to result from the fact that both IR and radio emissions are related to short-lived massive stars: the former originates from dust heated by ultraviolet (UV) light from blue, massive stars and the latter from synchrotron emission of electrons produced in supernova remnants. Therefore, a relation consistent with the local one is an indication of star formation dominating both the IR and radio emissions. There is growing evidence that the correlation holds at redshifts $z \lesssim 1$ (Garrett, 2002; Gruppioni et al., 2003; Appleton et al., 2004; Boyle et al., 2007; Marleau et al., 2007; Vlahakis et al., 2007; Yang et al., 2007). At higher redshifts sample sizes are small making it difficult to draw robust conclusions (Appleton et al., 2004; Kovács et al., 2006; Beswick et al., 2008; Ibar et al., 2008; Sajina et al., 2008; Garn et al., 2009; Murphy et al., 2009; Murphy, 2009; Rieke et al., 2009; Seymour et al., 2009; Younger et al., 2009b). The only sign of evolution was reported by Ivison et al. (2009) based on stacking analysis of the $24\ \mu\text{m}$ -selected galaxies, though possibly interpreted as a selection effect.

The objective of this paper is to model for the first time the entire UV-to-radio spectral energy distributions of a statistically significant sample of SMGs in a self-consistent way. Using these models we *i*) consistently derive the properties of SMGs using all available data to characterize their nature and determine the dominant emission mechanism; *ii*) estimate the contribution of SMGs to the cosmic SFR and stellar mass densities; *iii*) investigate whether the local IR-radio correlation holds at high redshifts in an unchanged form. In Section 2 our SMG sample is presented. Our methodology is outlined in Section 3. We derive the properties of SMGs in Section 4 and discuss the implications in Section 5. Section 6 closes with our conclusions. We use a cosmological model with $H_0 = 70\ \text{km s}^{-1}\ \text{Mpc}^{-1}$, $\Omega_\Lambda = 0.7$ and $\Omega_m = 0.3$.

2. Sample

We base our analysis on 76 SMGs ($S_{850} \gtrsim 3\ \text{mJy}$) from the sample of Chapman et al. (2005), all with spectroscopically measured redshifts spanning a range of 0.080–3.623.

The way the sample is selected involves complex biases, which are difficult to fully quantify and account for. The parent sample of Chapman et al. (2005) consists of 150 SMGs out of which 104 have radio identifications. The sample discussed here (76 galaxies) consists of the SMGs for which redshifts have been measured (spectroscopic completeness $\sim 75\%$). All this implies that the sample is biased against: *i*) faint submillimeter emitters (low dust content and/or hot dust, influence mostly the low- z portion of the sample); *ii*) faint radio emitters (high- z and cold dust, see

Figure 3 of Chapman et al., 2005); *iii*) faint optical emitters (difficult to obtain spectra); *iv*) $z \sim 1.2$ – 1.8 (“redshift desert” where no emission lines enter the observable wavelengths). At low redshifts ($z < 1$) the sample may also be incomplete due to a limited sky area (and therefore – volume) coverage making it difficult to detect rare strong submillimeter emitters (for details on the SMG selection effects see also Figure 2 of Blain et al. (2004) and discussion in Section 4.4 of Michałowski et al. (2008)).

It is important to estimate what the influence of these selection effects on our results is. In total we analyse $\sim 50\%$ (76/150) of the parent sample. Additionally, 25 radio-detected SMGs without spectroscopic redshifts have similar long-wavelength properties compared to the redshift sample (see Figure 1 of Chapman et al., 2005), so their absence from the sample probably does not significantly bias our results. The same is true for the SMGs in the “redshift desert”, since they are missed not due to their inherent properties. The remaining 46 radio-nondetected SMGs ($\sim 30\%$) could in principle have very different properties than our sample resulting in a potential limitation in our analysis.

Even if most of the SMGs without spectroscopic redshifts are similar to those in our sample, the incompleteness at $z < 1.8$ implies that the estimates of SMG densities (Sections 5.3.1, 5.3.2 and 5.2.3) in the three low-redshift bins (see Section 3.2) are strict lower limits.

Due to the negative K-correction at submillimeter wavelengths, SMGs at $z \gtrsim 0.5$ form a sample with homogeneous IR luminosity (Blain & Longair, 1996; Blain, 1997). However, SCUBA sources at $z \lesssim 0.5$ belong to a different population of objects and are intrinsically fainter. The limited volume coverage at these low redshifts makes the sample of these objects small and incomplete. This prevents a separate study of their properties. We did not take into account these sources when we computed median values of the properties of SMGs.

The photometric datapoints (Tables A.1 and A.2 in appendix¹) were collected from the literature: Ivison et al. (2002, *IK*, radio), Ivison et al. (2005, *R*, 1.2 mm), Chapman et al. (2003b, *VI*), Chapman et al. (2005, *BR*, 850 μm , radio), Capak et al. (2004, *UBVRIzHK*), Clements et al. (2004, *UBVIK*), Egami et al. (2004, 24 μm), Greve et al. (2004, 1.2 mm), Smail et al. (2004, *IJK*), Fomalont et al. (2006, *Rz*), Kovács et al. (2006, 350 μm , 1.2 mm), Laurent et al. (2006, 350 μm , 1.1 mm), Tacconi et al. (2006, 1.3 mm), Pope et al. (2006, *R*, 24 μm), Huynh et al. (2007, 160 μm), Hainline (2008, 3.6, 4.8, 5.6, 8.0, 24, 70 μm). We have not used the existing mid-IR spectra (Valiante et al., 2007; Pope et al., 2008; Menéndez-Delmestre et al., 2007, 2009), but for completeness we have indicated in Table A.1 those SMGs for which *Spitzer*/IRS spectra exist.

3. Methodology

3.1. SED modeling

In order to model the spectral energy distributions (SEDs) of SMGs, we use all the photometric datapoints simultaneously. This has the advantage that all the galaxy properties

¹ For convenience we make the compilation available in electronic form. We suggest that the original data source be consulted and referred to appropriately.

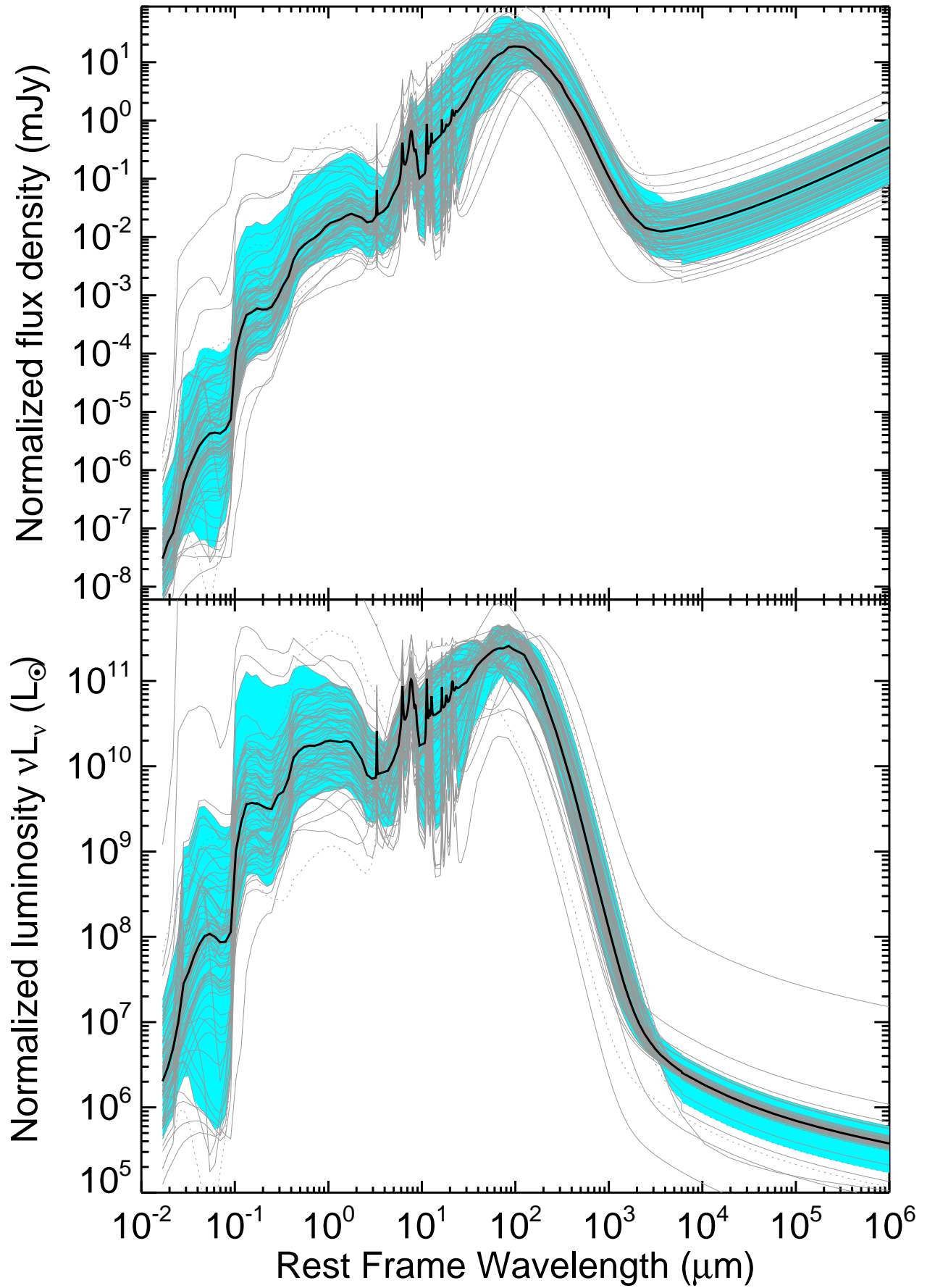


Fig. 1 Median spectral energy distribution (SED) of SMGs (*thick lines*) and SEDs of individual SMGs (*thin lines*). *Dotted lines* indicate $z < 0.5$ objects. *Shaded areas* enclose 90% of the SEDs. *Top*: all SEDs were divided by the corresponding $850 \mu\text{m}$ datapoint and scaled, so that the median SED has a flux of 5 mJy at the rest-frame $283 \mu\text{m}$ (observed $850 \mu\text{m}$ at $z = 2$). *Bottom*: SEDs were normalized to an infrared star formation rate of $100 M_{\odot} \text{ yr}^{-1}$.

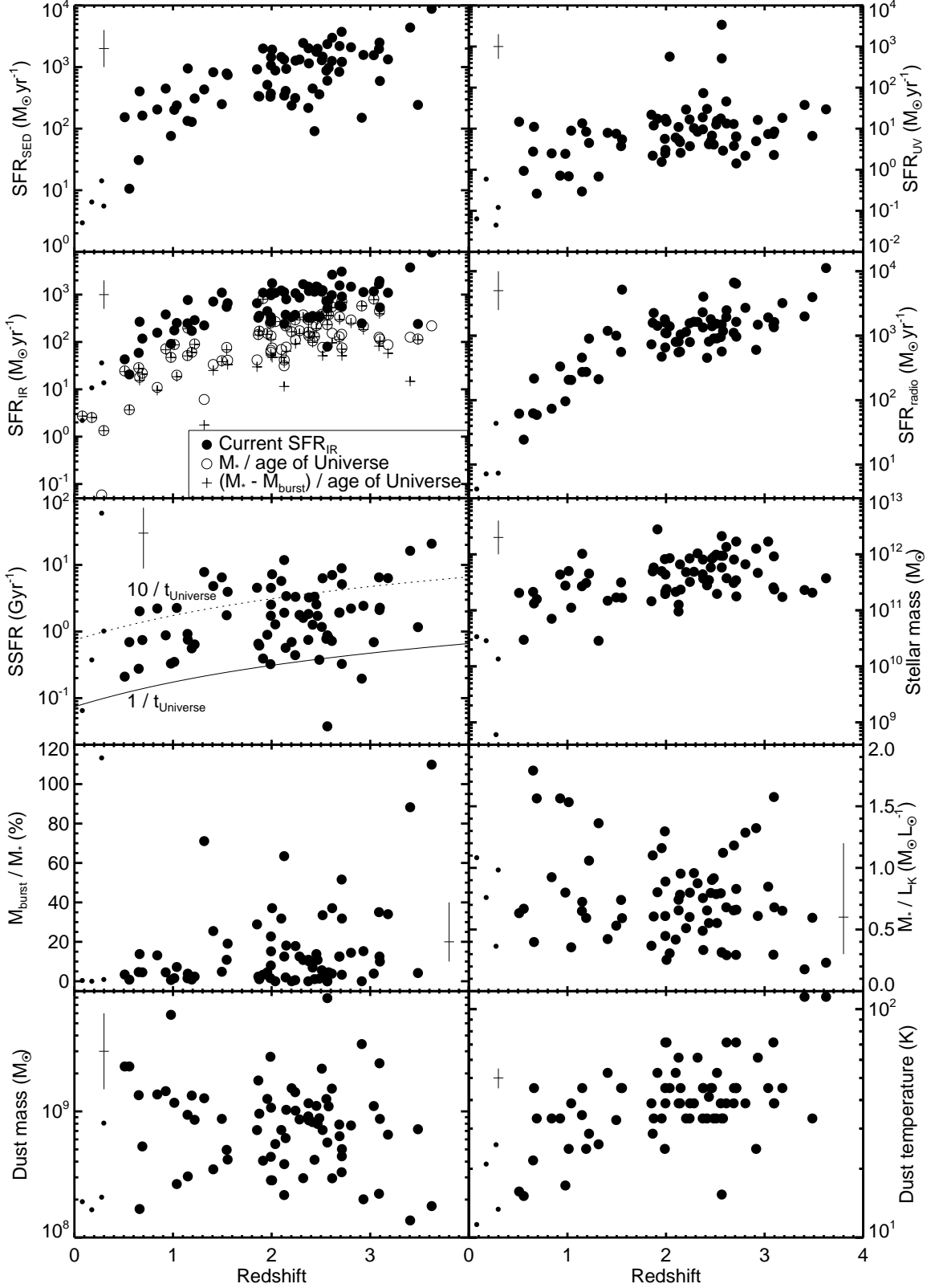


Fig. 2 Redshift evolution of the properties (*full circles*, see Table A.3 in appendix) of the sample of 76 SMGs with spectroscopic redshifts (Chapman et al., 2005). *Small symbols* indicate $z < 0.5$ objects. Typical errors (Section 4) are shown as *crosses*. From top-left to bottom-right: star formation rate (SFR) derived from spectral energy distribution modeling, ultraviolet, infrared and radio emission, SFR per unit stellar mass ($\equiv \text{SFR}_{\text{IR}}/M_*$), stellar mass, fraction of stellar population formed during the ongoing starburst, stellar mass-to-light ratio, dust mass and temperature. In the SFR_{IR} panel, we also show the minimum average SFRs (see Section 5.2.1) required to build up the total stellar mass within the age of the Universe at a given redshift (*empty circles*) and to build up the fraction of stellar population that was not formed during the ongoing starburst (*plus signs*). The location of plus signs indicates that SMGs must have been highly star-forming even before the onset of the ongoing starburst. When empty circles and plus signs overlap, the contribution of the ongoing starburst to the total stellar mass of a galaxy is negligible (i.e. $M_{\text{burst}}/M_* \sim 0$).

are derived consistently regardless of the wavelength regime in which those properties shape the SEDs (for example, recent star formation governs the UV and far-IR parts of a spectrum of a galaxy, whereas accumulated stellar mass is responsible for near-IR emission). Moreover in the full SED modeling no single datapoint drives the fit alone.

We utilized the set of 35000 models from Iglesias-Páramo et al. (2007) developed in GRASIL (Silva et al., 1998)² based on numerical calculations of radiative transfer within a galaxy. They cover a broad range of galaxy properties from quiescent to starburst. Their star formation histories are assumed to be a smooth Schmidt-type law (SFR proportional to the gas mass to some power, see Silva et al., 1998, for details) with a starburst (if any) on top of that starting 50 Myr before the time of the evolution of a galaxy at which the SED is computed. Additionally we fitted templates based on nearby galaxies (Silva et al., 1998) and gamma-ray burst host galaxies (Michałowski et al., 2008). We simultaneously used all the photometric datapoints from UV to radio (Tables A.1 and A.2). In cases where the data given by different authors were contradictory, we disregarded the obvious outliers. We scaled the SEDs to match the data and chose the one with the lowest χ^2 .

Based on the best fits we derived the properties of the galaxies as explained in Michałowski et al. (2008, 2009). In particular, SFRs, stellar (M_*) and starburst (M_{burst}) masses were given as output from GRASIL, rest-frame UV and K (L_K) monochromatic luminosities were interpolated from the best-fitting SEDs, whereas IR luminosities (L_{IR}) were integrated in a range 8–1000 μm , UV and IR SFRs (SFR_{IR} was adopted for all subsequent calculations, because SFR_{UV} is on average two orders of magnitude lower) were calculated using Kennicutt (1998), dust masses (M_d) were calculated from the 850 μm detections using equation (5) of Michałowski et al. (2009) and radio SFRs were calculated from the 20 cm detections using the empirical formula of Bell (2003) (see Section 4.2 of Michałowski et al., 2009). Dust temperatures (T_d) were estimated by identifying the peak of the dust emission and assuming an emissivity index $\beta = 1.3$. The average extinction in the rest-frame V -band was calculated from the unextinguished starlight given in GRASIL: $A_V = 2.5 \log(\text{unextinguished } V\text{-band starlight} / \text{observed } V\text{-band starlight})$. IR-radio correlation parameters were calculated according to the formula $q = \log(L_{\text{IR}}[L_\odot]/3.75 \times 10^{12}/L_{\nu 1.4\text{GHz}}[L_\odot\text{Hz}^{-1}])$, where $L_{\nu 1.4\text{GHz}}$ is a rest-frame 1.4 GHz luminosity density computed from the observed 1.4 GHz flux assuming a spectral slope of -0.75 .

3.2. Volume densities

In order to calculate the SFR density, the stellar density and the dust mass densities per unit comoving volume, ρ_{SFR} , ρ_* and ρ_{dust} , we used the following angular areas for the submillimeter surveys (Table 1 of Chapman et al., 2005): CFRS-03: 60 arcmin² and CFRS-14: 48 arcmin² (Webb et al., 2003b), Lockman Hole: 122 arcmin² and ELAIS-N2: 102 arcmin² (Scott et al., 2002), HDF-N: 100 arcmin² (Chapman et al., 2001), SSA-13 and SSA-22: 100 arcmin² each (Chapman et al., 2003a), totaling 632 arcmin².

We divided our sample into four high-redshift bins (Table 1) with approximately the same number of SMGs plus an additional bin for $z < 0.5$ sources (see Section 2). The densities in each bin were calculated as a sum of SFR_{IR} (or M_* , or M_d) of all SMGs in this bin divided by its comoving volume (a similar approach to calculate the SFR and number volume densities of SMGs was taken by Coppin et al., 2009; Daddi et al., 2009b; Younger et al., 2009a; Wang et al., 2009). The volume densities (Column 2) were found using the total area from the previous paragraph.

We removed the contribution of ten SMGs³, which were observed by SCUBA in the photometry mode (as opposed to the blank-field mapping mode) targeting optically-faint radio galaxies (Chapman et al., 2005). These objects fall outside the fields discussed here.

The method is therefore to analyse the fraction of the sky observed by SCUBA and estimate the number of SMGs and their volume densities. However, the true number of SMGs in our fields could be higher. On the other hand, regardless of the selection effects, the true number of SMGs in our fields cannot be lower than the number of SMGs in our sample. In turn, the true values of SFR and M_* densities cannot be lower than the values we derive. Therefore our results on volume densities should be regarded as robust lower limits.

Having this in mind we note that the parent sample of Chapman et al. (2005) includes only 29% of all the SMGs detected in the used survey fields (compare with Scott et al., 2002; Webb et al., 2003b,a). Therefore even if we analysed the full parent sample the estimated densities would be conservative lower limits. We attempt to correct for this incompleteness by assuming that the parent sample of Chapman et al. (2005) is a fair representation of the total population. In this case our numbers should be multiplied by 3.5 ($\sim 1/29\%$). This correction should in principle be derived separately for each redshift bin, but the missing redshift information for the majority of the SMGs in the used survey fields makes such calculation impossible. We note that this correction does not remove the bias against SMGs that are faint at radio and optical wavelengths, as discussed in Section 2.

We have not applied a volume density correction for the AGN contribution, because it is at most minor. Even though a fraction of SMGs host AGNs and a few individual SMGs have been shown to exhibit a significant AGN contribution to their emission, it is established that on average AGN activity is responsible for at most $\sim 10\text{--}20\%$ of the bolometric infrared emission of SMGs (Alexander et al., 2005, 2008; Menéndez-Delmestre et al., 2007, 2009; Valiante et al., 2007; Pope et al., 2008; Hainline et al., 2009; Murphy et al., 2009; Watabe et al., 2009). Therefore a potential error associated with the AGN contribution in our analysis of a statistically significant sample is smaller than the systematic uncertainty (e.g. 30% error of luminosity-SFR conversion; Kennicutt, 1998).

The percentage contribution of SMGs to the SFR and M_* densities (Columns 5 and 7 of Table 1) was calculated as

³ SMMJ123553.26+621337.7, SMMJ123555.14+620901.7,
SMMJ123600.10+620253.5, SMMJ123600.15+621047.2,
SMMJ123606.85+621021.4, SMMJ123716.01+620323.3,
SMMJ163706.51+405313.8, SMMJ221804.42+002154.4,
SMMJ221806.77+001245.7

² <http://adlibitum.oat.ts.astro.it/silva/default.html>

$\rho_{\text{SMG}}/(\rho_{\text{SMG}} + \rho_{\text{other}})$, where ρ_{SMG} is the density of SMGs at each redshift bin (Columns 4 and 6) and ρ_{other} is the density of other galaxies assumed to be an average of determinations (excluding lower limits) reported by other authors (Figure 4; Tables A.4 and A.5 in appendix), for which the redshift ranges overlap with our bins. This way of calculating the contribution is justified if SMGs do not enter the “other” samples of galaxies. This is usually the case because SMGs are faint in the optical. However, if this was not fulfilled, the real percentage contribution of SMGs would be even higher.

4. Results

The best fits⁴ are shown in Figure A.1 and the median SEDs (in flux and luminosity domains) are shown in Figure 1.

The resulting properties of the galaxies are listed in Table A.3 and shown in Figure 2 as a function of redshift. We notice similar trends to Hainline (2008) that lower- z SMGs are less luminous and colder (see her Figures 4.7 and 4.9).

In two cases we obtained much better fits using the templates of Silva et al. (1998) instead of those of Iglesias-Páramo et al. (2007), namely, an HR 10 template for SMMJ105151.69+572636.0 and a spiral Sc template for SMMJ221733.12+001120.2. In 9 cases⁵ where our fits strongly underpredict the 850 μm datapoint we adopted the L_{IR} and T_d estimates of Chapman et al. (2005).

The determination of the IR luminosity suffers from systematic uncertainties depending on the choice of the SED template. Our approach of using all the optical, submillimeter and radio data to constrain the shape of the SED results in a moderate systematic error in the IR luminosity (less than a factor of ~ 2 ; Bell et al., 2007). The choice of a Salpeter (1955) IMF with cutoffs of 0.15 and 120 M_{\odot} introduces a maximum systematic error of a factor of ~ 2 in the determination of the stellar masses and SFRs (Erb et al., 2006). Bell et al. (2007) have also found that random errors in stellar mass are less than a factor of ~ 2 . Estimates of dust temperatures have uncertainties of ~ 5 – 10 K dominated by the unknown value of the emissivity index, β . The SFR determination based on radio observations is accurate up to 30% since it agrees with the detailed spectrophotometric SED fitting (Michałowski & Hjorth, 2007). The uncertainties in q (defined in Section 3.1) are ~ 0.3 (see also Kovács et al., 2006), dominated by the error in L_{IR} .

In order to assess the influence of the choice of emissivity index $\beta = 1.3$ on the dust mass estimates, we recalculated the dust temperatures and masses in a range of β of 1–2. The resulting error was less than a factor of 3.5.

This is illustrated on Figure 3 where we present a more systematic analysis of this problem. We calculated the dust mass of a mock galaxy with $T_d = 40$ K (this choice does not influence the results) using β in the range 1–2 assuming a flux density of 5 mJy at a variety of infrared rest-wavelengths probed by observations. Then we normalized

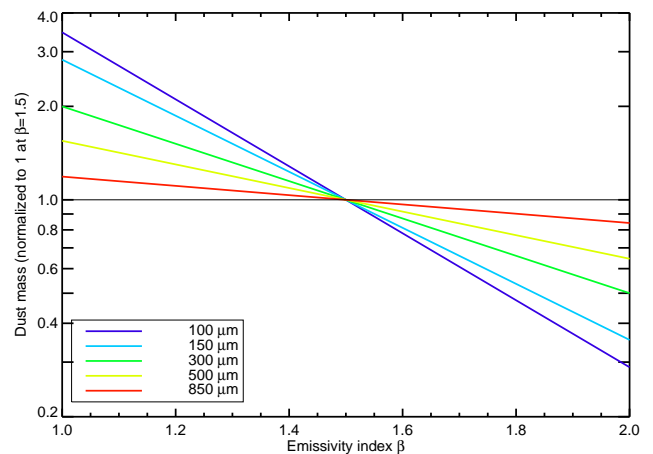


Fig. 3 Derived dust mass of a mock galaxy with dust temperature $T_d = 40$ K and a flux density of 5 mJy at several infrared rest-wavelengths as a function of the assumed emissivity index β . For each wavelength the dust masses were normalized to 1 at $\beta = 1.5$. The spread of the derived dust masses shows that the uncertainty of the dust mass resulting from unknown β is a factor of a few.

dust masses to 1 at $\beta = 1.5$. We conclude that as long as the observations probe wavelengths longer than ~ 150 μm ($z \lesssim 4.7$ for observed wavelength of 850 μm), then the error on the dust mass resulting from unknown β is less than a factor of ~ 5 .

None of these errors significantly affects our conclusions, because the inferred nature of SMGs would not be different even in the worst case scenario when all systematic errors work in one direction (increasing or decreasing the obtained values). Moreover, we analyse a statistically significant sample of 76 galaxies, so random errors of a factor of 2 are reduced to $< 20\%$ when an error of a mean is considered.

Table 1 contains the volume densities and mean IR-radio correlation parameter divided into five redshift bins (see Section 3.2). The uncertainties quoted on ρ_{SFR} and ρ_* include the systematic 30% uncertainty of the L_{IR} to SFR conversion (Kennicutt, 1998) and a factor of ~ 2 systematic uncertainty in the stellar mass (Michałowski et al., 2008). The systematic error resulting from our incompleteness correction (Section 3.2) is likely a factor of a few.

5. Discussion

5.1. Spectral energy distributions of SMGs

We have presented the first successful attempt to fit the entire UV-to-radio SEDs of SMGs in a self-consistent way taking into account all the available data simultaneously. Our study provides evidence that GRASIL models can reproduce the SMG data. Namely, we found good fits for all SMGs in our sample with the best IR/submillimeter wavelength coverage⁶ except of SMMJ105238.30+572435.8.

As is evident from Figure 1, regardless of whether SEDs were normalized to the same observed 850 μm datapoint

⁴ The SED fits can be downloaded from <http://archive.dark-cosmology.dk>

⁵ SMMJ030226.17+000624.5, SMMJ030231.81+001031.3,
SMMJ030236.15+000817.1, SMMJ030238.62+001106.3,
SMMJ123636.75+621156.1, SMMJ123651.76+621221.3,
SMMJ123721.87+621035.3, SMMJ163639.01+405635.9,
SMMJ221724.69+001242.1

⁶ SMMJ105201.25+572445.7, SMMJ105230.73+572209.5,
SMMJ163650.43+405734.5, SMMJ163658.19+410523.8,
SMMJ163706.51+405313.8

Table 1 Mean values for SMGs in redshift bins

z	Volume (10^6 Mpc^3)	$\log \rho_{\text{IR}}$ ($L_{\odot} \text{ Mpc}^{-3}$)	ρ_{SFR} ($M_{\odot} \text{ yr}^{-1} \text{ Mpc}^{-3}$)	%	$\log \rho_{*}$ ($M_{\odot} \text{ Mpc}^{-3}$)	%	q	$\log \rho_{\text{dust}}$ ($M_{\odot} \text{ Mpc}^{-3}$)
(1)	(2)	(3)	(4)	(5)	(6)	(7)	(8)	(9)
0.080 – 0.500	0.12	$7.03^{+0.11}_{-0.14}$	0.0018 ± 0.0005	5^{+3}_{-2}	$6.35^{+0.21}_{-0.16}$	$1^{+0.4}_{-0.2}$	2.54 ± 0.12	$4.06^{+0.05}_{-0.06}$
0.510 – 1.316	1.03	$7.81^{+0.06}_{-0.07}$	0.0111 ± 0.0016	9^{+2}_{-2}	$7.16^{+0.13}_{-0.08}$	5^{+2}_{-1}	2.52 ± 0.06	$4.32^{+0.04}_{-0.05}$
1.408 – 2.142	1.63	$8.12^{+0.05}_{-0.05}$	0.0228 ± 0.0027	11^{+3}_{-3}	$7.18^{+0.16}_{-0.11}$	11^{+6}_{-3}	2.29 ± 0.08	$3.84^{+0.04}_{-0.04}$
2.148 – 2.565	0.89	$8.45^{+0.05}_{-0.05}$	0.0486 ± 0.0054	18^{+7}_{-5}	$7.61^{+0.12}_{-0.08}$	51^{+20}_{-11}	2.27 ± 0.09	$4.35^{+0.04}_{-0.04}$
2.578 – 3.623	2.17	$8.30^{+0.05}_{-0.05}$	0.0341 ± 0.0040	20^{+5}_{-4}	$7.28^{+0.12}_{-0.07}$	31^{+14}_{-7}	2.25 ± 0.08	$3.86^{+0.03}_{-0.03}$

Note. — Column (1): redshift range of the bins. Column (2): comoving volume of these bins (calculated in Section 3.2). Column (3): IR luminosity density of SMGs. Column (4): Resulting IR SFR density of SMGs (Section 5.3.1). Column (5): contribution of SMGs to the cosmic SFR density (calculated in Section 3.2). Column (6): stellar mass density of SMGs (Section 5.3.2). Column (7): contribution of SMGs to the cosmic M_{*} density (calculated in Section 3.2). Column (8): mean (and error of the mean) FIR-radio correlation parameter for SMGs (Section 5.4.1). Column (9): dust mass density of SMGs (Section 5.2.3). Columns 3-7 and 9 have been corrected for incompleteness by a factor of 3.5 (Section 3.2).

or SFR_{IR} , the scatter at optical and near-IR wavelengths is significant, showing that SMGs exhibit a wide range of stellar population properties (as also noted by Ivison et al., 2002). This implies the need for an SED template library in SMG studies, as opposed to single-template fitting.

Having constrained the SEDs of SMGs we now turn to a discussion of what we can learn about these galaxies using the best-fitting models.

5.2. Properties of SMGs

5.2.1. Star formation rates

The very high (current) SFRs of SMGs (median $713 M_{\odot} \text{ yr}^{-1}$, Column 5 of Table A.3 and Figure 2) place them among the most powerful starburst galaxies in the Universe. Such extreme SFRs likely result from major mergers (e.g. Chapman et al., 2004; Swinbank et al., 2004; Greve et al., 2005; Tacconi et al., 2006, 2008; Younger et al., 2007, 2008; Berciano Alba et al., 2010; Narayanan et al., 2009, 2010) and cannot be sustained for a long period (after a few hundred Myr at most the gas reservoir should be depleted; see Greve et al., 2005; Hainline et al., 2006).

On the other hand, their extinction-uncorrected UV SFRs are two orders of magnitude lower (median $\sim 7 M_{\odot} \text{ yr}^{-1}$, Column 4). This implies that the majority of star formation in SMGs is hidden by dust. Therefore, optical observations alone are not sufficient to investigate their nature and contribution to cosmic star formation.

Using stellar masses of SMGs we placed lower limits on the time-averaged SFRs required to build their stellar masses within the age of the Universe ($\equiv M_{*}/\text{age}$ of the Universe at given redshift), shown as empty circles on Figure 2. Their median value of $\sim 130 M_{\odot} \text{ yr}^{-1}$ indicates that SMGs had to be relatively highly star-forming throughout the age of the Universe to build up their stellar populations at a constant rate. Even if our estimates of stellar masses were underestimated by a factor of a few due to systematic uncertainties (Section 4), the SMGs would have had to be luminous infrared galaxies (LIRGs with $\text{SFR} \gtrsim 20 M_{\odot} \text{ yr}^{-1}$) during their evolution.

Having constrained the mass of stars formed during the ongoing starburst episode, M_{burst} , we can further constrain the minimum average SFR of SMGs *before* the onset of this

starburst, $\equiv (M_{*} - M_{\text{burst}})/\text{age}$ of the Universe (plus signs on Figure 2). The median is still high, $\sim 100 M_{\odot} \text{ yr}^{-1}$, so SMGs must have been highly star-forming in the past too. At redshifts 2–3 the age of the Universe is $\sim 3\text{--}2$ Gyr and it is unlikely that a galaxy can sustain this high SFR over such a long period. *Therefore we conclude that either the stellar masses of SMGs have been formed in at least two strong ($> 100 M_{\odot} \text{ yr}^{-1}$) starburst episodes or continuously over the period of 2-3 Gyr but in several smaller galaxies that eventually merged.* In order to build up the stellar mass of one SMG, five such galaxies would need to form stars continuously at a rate of $20 M_{\odot} \text{ yr}^{-1}$, a value more likely to be sustainable over several Gyr. The latter scenario is consistent with the results of Dye et al. (2008) based on observed optical to mid-IR data of 51 SMGs with photometric redshifts. They found that approximately half the stellar mass in SMGs has been formed over a long ($\sim 1\text{--}2$ Gyr) period of approximately constant star formation activity. The possibility that a significant part of stellar mass in SMGs was formed before the ongoing starburst has also been suggested by Hainline (2008), who compared the build-up timescale of stellar mass and the duration of the SMG phase.

The median value of the SFR per unit stellar mass ($\text{SSFR} \equiv \text{SFR}_{\text{IR}}/M_{*}$, Column 7 of Table A.3) of $\sim 1.8 \text{ Gyr}^{-1}$ is within the range for other high- z star-forming samples (compare with Figures 2 and 4 of Castro Cerón et al., 2006, 2009, respectively). This indicates that SMGs are forming stars intensely.

SSFRs are compared with (the inverse of) the age of the Universe in Figure 2. The SMGs close to the solid line could have formed their stellar populations at the present rate within the age of the Universe. However, the SMGs close to, or above the dashed line could have formed their stars at the present rate within less than 10% of the age of the Universe, i.e., within $\lesssim 300$ Myr at $z = 2$. These galaxies are experiencing a powerful starburst episode.

At the extreme there are three high- z SMGs⁷ with very high SSFRs $> 10 \text{ Gyr}^{-1}$ (Column 7 of Table A.3). They are all hot ($T_d > 60$ K, Column 13) and formed the majority of their stellar populations during the ongoing starburst

⁷ SMMJ131201.17+424208.1, SMMJ141802.87+523011.1, SMMJ221806.77+001245.7 plus a low-mass, low- z case, SMMJ030238.62+001106.3

($M_{\text{burst}}/M_* > 60\%$, Column 9). Therefore they are likely the most powerful cases of SMGs formed in major mergers of galaxies with huge gas reservoirs that were subsequently converted into stars.

Our median SSFR at $z > 1.7$ (1.83 Gyr^{-1}) is a factor of ~ 2 lower than that of Dunne et al. (2009, $3\text{--}4.5 \text{ Gyr}^{-1}$; see their Figure 12b) for $10^{11} < M_* < 10^{12} M_\odot$ galaxies at these redshifts. This difference can be explained if the radio luminosities (used by Dunne et al., 2009, to estimate SFRs) are boosted by AGN activity more than the IR luminosities used here. Indeed, if we use $\text{SFR}_{\text{radio}}$ instead of SFR_{IR} to calculate SSFRs the median for the SMGs at $z > 1.7$ increases to 3.20 Gyr^{-1} (see Section 5.4.2 for discussion of AGN contamination in our sample).

In order to assess the accuracy of SFR estimates based on radio emission (independent of SED modeling) we compared the ratio of $\text{SFR}_{\text{radio}}/\text{SFR}_{\text{IR}}$. Its median value is equal to ~ 1.3 . Hence, assuming that IR emission is a good proxy for SFR, then radio estimates suffer from a $\sim 30\%$ systematic error. This is illustrated on Figure 5 where the dashed line denotes the relation between IR and radio luminosities required to make $\text{SFR}_{\text{IR}} = \text{SFR}_{\text{radio}}$. Indeed the radio luminosity gives systematically higher SFRs for SMGs (most of the points are above the line). This can be caused by a significant AGN contamination boosting radio flux (see Section 5.4.2), or a strong bias favouring radio-bright galaxies, because those non-detected at radio do not enter our sample (Section 2). Alternatively, it could be that for luminous galaxies either the IR conversion of Kennicutt (1998) should be scaled up by a factor of 1.3, or the radio conversion of Bell (2003) scaled down.

5.2.2. Stellar masses

SMGs having stellar masses of $\sim 10^{11}\text{--}10^{12} M_\odot$ (Column 8 of Table A.3 and Figure 2) are among the most massive galaxies in the Universe, regardless of redshift (compare with Figures 2 and 4 of Castro Cerón et al., 2006, 2009, respectively). This property makes them natural candidates for the progenitors of the present-day ellipticals.

The relatively tight range of stellar masses is likely not a result of sensitivity limits at optical and near-IR. This is because *i*) galaxies with stellar mass as low as $\sim 10^9 M_\odot$ would have been detected in deep *Spitzer* imaging at redshifts $z \sim 2$ (e.g. Reddy et al., 2006) *ii*) our sample accounts for 50% of the parent Chapman et al. (2005) sample (and only 30% of the parent sample may have different properties than our sample, see Section 2), so it is unlikely that we miss only the low-mass objects. Therefore, high M_* seems to be an intrinsic property of submillimeter-selected galaxies. Mergers of less massive galaxies could not result in a powerful starburst giving rise to detectable submillimeter emission (see also Davé et al., 2009).

Only a minor part (median $\sim 8\%$, Column 9 of Table A.3 and Figure 2) *of the stellar populations present in SMGs has been formed during the ongoing starburst episodes.* Hence, even though SMGs probably evolve into ellipticals, the majority of the stellar mass in such ellipticals had been created before the submillimeter-bright phase.

This could mean that the current SFRs and stellar masses of SMGs are only loosely connected and indeed this manifests itself in a very high spread (around two orders of magnitude) in SSFRs in our sample even though the stellar

mass range is relatively tight: $\sim 10^{11}\text{--}10^{12} M_\odot$ (Figure 2). This behaviour is unusual compared to other galaxies (see Castro Cerón et al., 2006, 2009).

However we note that the low stellar masses created in the ongoing starburst may partially be an effect of the assumed starburst ages of 50 Myr. If a starburst duration of 100–200 Myr were adopted (Smail et al., 2004; Borys et al., 2005; Hainline, 2008; Tacconi et al., 2008) the resulting M_{burst} could be higher by a factor of $\sim 2\text{--}4$.

The mass-to-light ratios, M_*/L_K , of SMGs (Column 10 of Table A.3 and Figure 2) are typical for massive galaxies. Specifically, the median ($0.68 M_\odot L_\odot^{-1}$) is similar to the values for $M_* > 10^{11} M_\odot$ galaxies (Drory et al., 2004, their Table 1) and to simulated massive galaxies at $z \sim 1$ (Courty et al., 2007, their Figure 4).

5.2.3. Dust properties

Our fits suggest that SMGs are moderately dust-obscured with a median $A_V \sim 2$ mag (Column 14 of Table A.3). Our estimates are consistent within $1\text{--}2\sigma$ with the mean/median values obtained by Smail et al. (2004, $1.70\text{--}2.44$), Swinbank et al. (2004, 3.0 ± 1.0), Borys et al. (2005, 1.7 ± 0.2) and Hainline (2008, 1.7 ± 0.1) based on near-IR data. For individual SMGs we obtained systematically larger extinction (median difference of ~ 0.3 mag) than Hainline (2008). The difference may be accounted for if there is significant extinction even in *Spitzer* IRAC data.

The dust density of SMGs at $z < 0.5$ (Column 9 of Table 1) is approximately 3% of the total local ($0.013 < z < 0.18$) dust budget of $\log \rho_{\text{dust}} = 5.57^{+0.12}_{-0.17} M_\odot \text{ Mpc}^{-3}$ given by Driver et al. (2007) based on an assumed dust-to-light ratio. Therefore SMGs contribute very little to the dust budget at low redshifts.

In our sample of SMGs ρ_{dust} does not change significantly from $z \sim 3.6$ to $z \sim 0.5$. We do not detect any evolution of dust mass in SMGs across the entire redshift range (Figure 2). A constant dust mass density across redshifts 0–3.5 was also found by Pascale et al. (2009) based on a stacking analysis at submillimeter wavelengths of galaxies selected at $24 \mu\text{m}$.

The question is what happened to the dust produced in SMGs. If they evolve into dust-poor ellipticals, then the dust is not simply stored in their end-products (as is probably the case for stellar masses). It is therefore plausible that dust is either blown away (by stellar and/or AGN winds) or absorbed in star formation, or destroyed during subsequent evolution after the SMG event.

5.2.4. Comparison with GRB hosts

In Michałowski et al. (2008) we presented a hypothesis that gamma-ray burst (GRB) host galaxies may constitute a subsample of hotter/less luminous counterparts of SMGs. Indeed, the UV-to-IR SEDs of three $z \sim 2\text{--}3$ SMGs⁸ are consistent with $z \sim 1$ submillimeter/radio bright GRB hosts (dashed lines on Figure A.1 from Michałowski et al., 2008), but 1.2–3.9 times more luminous. These three SMGs are similar to GRB hosts with respect to their hot dust temperatures ($\sim 40\text{--}60$ K), high SSFRs ($\gtrsim 2 \text{ Gyr}^{-1}$, high

⁸ SMMJ141750.50+523101.0, SMMJ141802.87+523011.1, SMMJ163627.94+405811.2

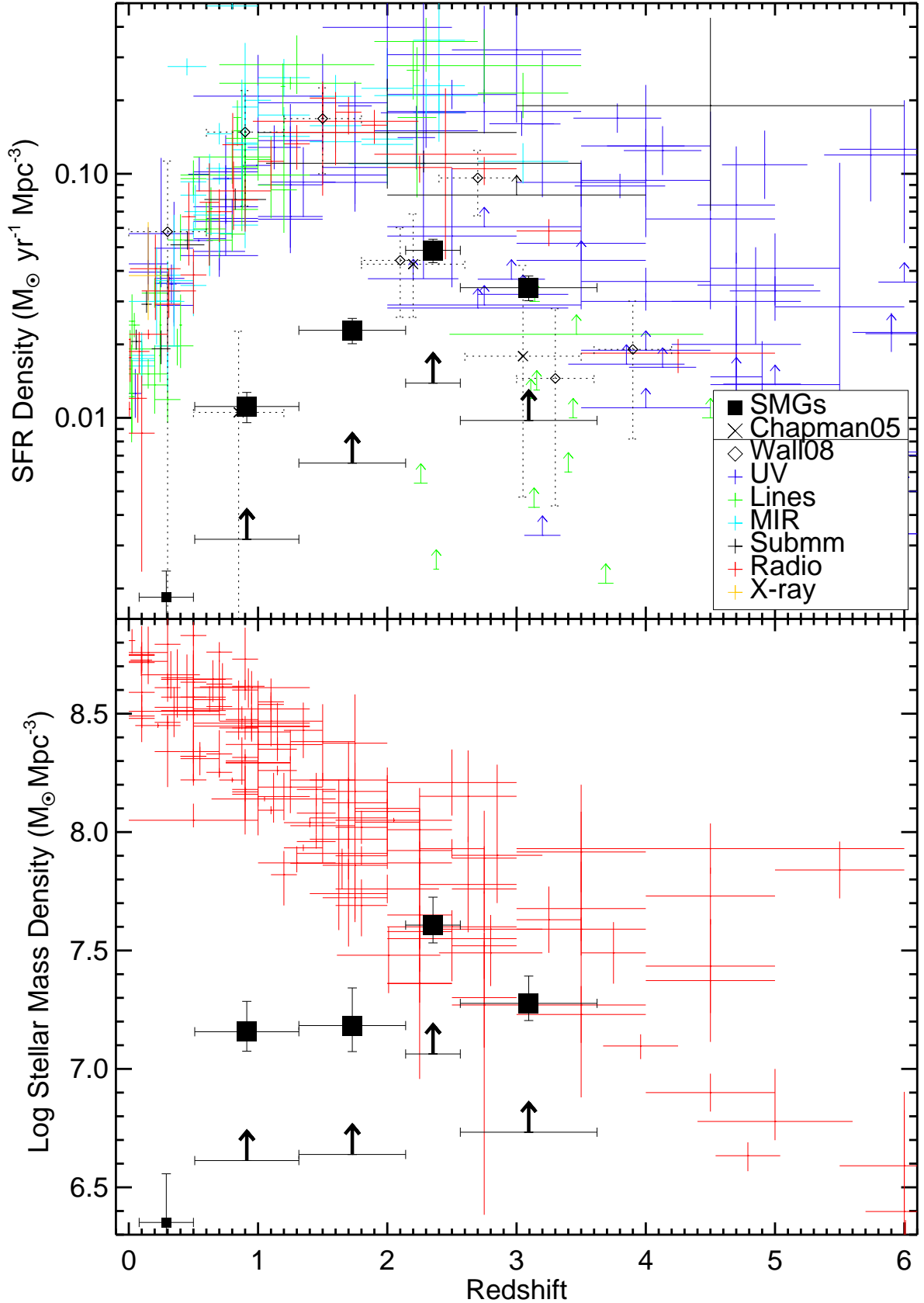


Fig. 4 *Top*: Cosmic star formation density. The SMGs' contribution rises with redshift from $\sim 9\%$ to $\sim 20\%$ (Section 5.3.1 and Table 1). *Filled Squares*: data for SMGs at $z > 0.5$ in four bins (Table 1 and Section 3.2). *Small Squares*: data for SMGs at $z < 0.5$. *Thick black arrows*: the SMG data without incompleteness correction (factor of 3.5, Section 3.2). *Black crosses and diamonds*: star formation density of SMGs determined by Chapman et al. (2005) and Wall et al. (2008), respectively. *Colored points with error bars*: determination of the cosmic value based on different estimates – ultraviolet (*violet*), emission lines: [O 2], [O 3], $H\alpha$, $H\beta$ (*green*), mid-IR (*light blue*), submillimeter (*black*), radio (*red*), X-ray (*yellow*). Extinction correction and, in many cases, incompleteness correction have been applied by the authors. *Arrows*: lower limits.

Bottom: Cosmic stellar mass density. The SMGs' contribution rises with redshift from $\sim 5\%$ to $\sim 50\%$ (Section 5.3.2 and Table 1). *Red points with error bars*: determination of the cosmic value from literature. The data and the references are listed in Tables A.4 and A.5 in appendix.

fraction of stellar mass formed in the ongoing starburst ($> 10\%$) and blue optical colors.

If larger samples of GRB hosts shows a similar tendency that their brightest members overlap with the hotter subsample of SMGs, then GRB events will provide an effective way of selecting hot SMGs, otherwise difficult to localize.

5.3. Contribution to stellar mass assembly

5.3.1. Star formation rate volume density

SFR densities of SMGs were calculated as described in Section 3.2. In order to assess the accuracy of our simplified method of dividing the sum of the SFRs of the detected SMGs by the total survey volume, we compare our estimates with those resulting from detailed calculation of the volume contribution of individual SMGs done by Chapman et al. (2005, based on the same sample as we analyse) and Wall et al. (2008, based on 35 SMGs in GOODS-N field of which 17 have spectroscopic redshifts). The comparison is shown in Figure 4. Our results in two high-redshift bins ($z > 2$) corrected for incompleteness (Section 3.2) are consistent with that of Chapman et al. (2005) and Wall et al. (2008). At lower redshifts we find values similar to Chapman et al. (2005), but an order of magnitude lower than Wall et al. (2008). Therefore we conclude that *i*) our method to calculate volumes is accurate, since it gives consistent results with other estimates; and *ii*) our sample is incomplete in the three low-redshift bins as anticipated in Section 2.

From Figure 4 (and Columns 4 and 5 of Table 1) it is apparent that a ρ_{SFR} of SMGs starts to decline (with cosmic time) earlier (about $z \sim 2$) than that of other galaxies ($z \sim 1$). More quantitatively, SMGs harbour $\sim 20\%$ of the cosmic ρ_{SFR} at $z \sim 2-3.6$ (Column 5), but their contribution drops to $\sim 9\%$ at $0.5 < z < 1.4$. It is likely that at lower redshifts, due to the decreased rate of mergers (e.g. Rawat et al., 2008; de Ravel et al., 2009), there are fewer galaxies left that can still sustain high SFRs to be detected at submillimeter wavelengths. However, part of the decrease of SMG ρ_{SFR} can be explained by the “redshift desert”, which makes it difficult to measure redshifts of $z \sim 1.2-1.8$ SMGs (see Section 2).

A high value of ρ_{SFR} of SMGs at $z \sim 2-3$ and the subsequent decline are consistent with the hypothesis that the SMG population is a manifestation of powerful starburst episodes evolving into the present-day ellipticals (as discussed in Section 5.2.2). In this scenario galaxies detected in the submillimeter at high- z do not enter the sample of SMGs at low- z because they have already evolved into passive galaxies. It has indeed been found that ellipticals contain old stars formed at $z \sim 1.5-4$ (Daddi et al., 2000; van Dokkum & Franx, 2001; van de Ven et al., 2003). The evolution of SMGs into ellipticals has also been claimed by several authors based on their luminosity function (Smail et al., 2004), huge luminosities (Eales et al., 1999) and gas reservoirs (Smail et al., 2002; Greve et al., 2005), strong clustering (Iverson et al., 2000; Almaini et al., 2003), space density and morphology (Barger et al., 1999; Lilly et al., 1999; Trentham et al., 1999; Swinbank et al., 2006) and evolutionary SED models (Takagi et al., 2004).

Knudsen et al. (2008b) analysed number counts of SMGs fainter than the SCUBA confusion limit, using those

behind clusters of galaxies magnified by lensing. They concluded that the integrated light produced by the SMGs brighter than 0.1 mJy (i.e. LIRGs and ULIRGs with roughly $L_{\text{IR}} > 8 \times 10^{10} L_{\odot}$ and $\text{SFR} > 15 M_{\odot} \text{ yr}^{-1}$) is comparable to the extragalactic background light (EBL) at $850 \mu\text{m}$ (see also Blain et al., 1999; Cowie et al., 2002). This means that these galaxies host the majority of the cosmic *obscured* star formation. Knudsen et al. (2008b) also found that sources brighter than 2.5 mJy (roughly the limit of the survey considered here) contribute $\sim 25\%$ to the EBL at $850 \mu\text{m}$ (see also Hughes et al., 1998; Barger et al., 1999; Wang et al., 2004; Coppin et al., 2006). Together with our results this implies that as much as $\sim 80\%$ ($4 \times 20\%$) of the cosmic star formation at $z \sim 2-3.6$ reside in SMGs brighter than 0.1 mJy. This is only true if the faint (< 2 mJy) SMGs have similar dust temperatures to the brighter ones. If they are colder (hotter) their submillimeter fluxes corresponds to lower (higher) SFRs (because it is calibrated to total IR emission) and therefore the total SMG population contribute less (more) than 80% to the cosmic ρ_{SFR} . This picture is however complicated, because based on stacking analysis it has been claimed that the distribution of the faint SMGs peaks at lower redshifts ($z < 1.5$; Wang et al., 2006; Serjeant et al., 2008).

Our overall conclusion is that the SMG population plays a significant role at redshifts $z \sim 2-4$, namely sources brighter than ~ 3 (0.1) mJy at $850 \mu\text{m}$ host 20% (80%) of cosmic star formation. Their contribution can however be lower in reality if very small (but numerous) galaxies are missed in all high- z flux-limited galaxy surveys. In such a case the total SFR density (color points on Figure 4) would be underestimated. To solve this issue much deeper surveys at high- z are necessary, either blank-field or for well-selected dwarf galaxy samples (e.g., GRB hosts or Ly α emitters).

Zheng et al. (2007) estimated ρ_{SFR} at $z \sim 0.9$ for massive galaxies ($M_{*} > 10^{11} M_{\odot}$) down to $R < 24$ mag (only $\sim 40\%$ of SMGs satisfy the latter criterion) equal to $0.0052^{+0.0020}_{-0.0021} M_{\odot} \text{ yr}^{-1} \text{ Mpc}^{-3}$. This value is only a factor of 2 lower than our estimate for the SMGs at $0.5 < z < 1.4$ (Table 1). Therefore, although SMGs do not host a major fraction of the cosmic SFR at these redshifts, they contribute significantly ($0.0102 / (0.0052 \times 0.6 + 0.0102) \sim 66\%$) to the SFR budget of massive galaxies.

5.3.2. Stellar mass volume density

Stellar mass densities of SMGs were calculated as described in Section 3.2. Figure 4 and Table 1 (Columns 6 and 7) show that at $z \sim 2-3.6$ a significant part ($\sim 30-50\%$) of the cosmic stellar mass had been formed in the progenitors of SMGs. At lower redshifts ρ_{*} of SMGs (and hence their contribution to the cosmic ρ_{*}) drops, likely because the majority of SMGs at higher redshifts had already evolved into passive galaxies at $z \sim 1.5$, and so dropped out of our submillimeter-selected sample. Moreover the sample is incomplete at $z \sim 1.2-1.8$ due to the “redshift desert” (see Section 2). This brings down the densities of SMGs in the low- z bins.

Since most of the stellar mass of SMGs has not been formed in the ongoing starburst (Section 5.2.2), their ρ_{*} reflects the integrated contribution of SMGs to the cosmic ρ_{SFR} . Therefore the relatively high contribution of SMGs

to the cosmic ρ_* in the last redshift bin ($\sim 31\%$, Column 7 of Table 1) means that SMGs play a non-negligible role in the cosmic stellar assembly even at $z > 3.6$. This can be tested by analysis of a sample of $z \gtrsim 4$ SMGs in a defined survey sky area (e.g. Michałowski et al., 2010; Younger et al., 2009a, note that these results are likely affected by cosmic variance). It has been confirmed that such distant SMGs exist (Capak et al., 2008; Knudsen et al., 2008a, 2010; Schinnerer et al., 2008; Coppin et al., 2009; Daddi et al., 2009b,a).

5.4. Source of emission

5.4.1. IR-radio correlation

With our full SED modelling of 76 SMGs we confirm the results of Hainline (2008) on the correlation between IR and radio luminosities. Figure 5 shows that SMGs follow a linear IR-radio correlation. The two outliers (with $q \sim 1.3$, see Section 5.4.2) are probably caused by AGN activity contributing significantly to radio luminosities. A linear fit gives:

$$\log(L_{\nu 1.4\text{GHz}}/L_{\odot}\text{Hz}^{-1}) = (0.95 \pm 0.07) \log(L_{\text{IR}}/L_{\odot}) - (14.3 \pm 0.8). \quad (1)$$

The slope is consistent (within errors) with unity, suggestive of the linear relation between $L_{\nu 1.4\text{GHz}}$ and L_{IR} at the high-end ($L_{\text{IR}} \gtrsim 10^{11} L_{\odot}$) of the galaxy luminosity function (a similar value of 1.064 ± 0.025 was found by Hainline, 2008).

The IR-radio correlation is usually quantified by the ratio of IR and radio luminosities, q (see Section 3.1). The mean q for SMGs (2.32 ± 0.04 , scatter: 0.34) is significantly lower than that of local star-forming galaxies (2.64 with a scatter of 0.26; Bell, 2003). Similar offsets were reported by Kovács et al. (2006), Murphy et al. (2009) and Murphy (2009) based on smaller samples of SMGs. *We conclude that at $z > 1.4$ SMGs have radio luminosities on average a factor of ~ 2.1 larger ($\Delta q \sim -0.32$) than what would result from the local relation.* The difference is significant at the level of 4–5 σ and can be explained in three ways.

Radio-loud AGNs have on average low q values (see e.g. Miller & Owen, 2001; Yun et al., 2001; Yang et al., 2007). If $\gtrsim 50\%$ of the radio emission of SMGs is powered by AGNs, then the radio luminosities of SMGs higher by a factor of ~ 2.1 can be accounted for. However, there are indications that SMGs are starburst-dominated (see Section 5.4.2), so we deem this explanation less likely.

Another explanation is that the radio excess is a result of the bias against radio-faint sources in our sample (see Section 2). This can be tested when a sample of SMGs with localizations (and hence redshifts) independent of radio detections is available (e.g. Daddi et al., 2009b,a; Knudsen et al., 2010; Weiß et al., 2009a).

The third possibility is that some properties influencing the IR or radio emission are intrinsically different for SMGs and local galaxies. The sample of Bell (2003) includes local normal, star-forming spiral and irregular galaxies, blue compact dwarfs, starburst galaxies and ULIRGs. Therefore the difference in the properties between this sample and such extreme galaxies as SMGs is expected. Such explanation was offered by Lacki et al. (2009) and Lacki & Thompson (2009). Their numerical modelling showed that cosmic-ray electrons in “puffy starbursts” (vertically and radially extended

galaxies with vertical scale heights ~ 1 kpc) experience weaker bremsstrahlung and ionization losses resulting in stronger radio emission. Indeed, there are indications that SMGs are extended on vertical scales of ~ 1 kpc (Lacki & Thompson, 2009; Tacconi et al., 2006, 2008; Genzel et al., 2008; Younger et al., 2008; Law et al., 2009), so we find this explanation probable.

The systematic uncertainties in the determination of L_{IR} (factor of $\lesssim 2$, Section 4) may in principle also explain the offset. However, we find this unlikely because similar offsets were found by other authors using different fitting methods (Kovács et al., 2006; Murphy et al., 2009; Murphy, 2009).

The q values for SMGs are shown in Figure 6 as a function of redshift. We do not detect any significant evolution across the redshift range 1.4–3.6. The only sign of evolution is that the mean q in the low-redshift bin ($0.5 < z < 1.4$) is above the value found at higher redshifts ($\sim 4\sigma$). This can be explained either by the contribution of reprocessed emission from low-mass stars (cirrus emission, e.g. Yun et al., 2001, and references therein) to the IR, or by the fact that at low redshifts SMGs are more similar to other local galaxies and do not exhibit large vertical scale heights characteristic for “puffy starbursts” (see above).

It is important to note that the derived linear IR-radio correlation for SMGs is not a consequence of the use of the SED templates (which were tuned to fulfill this correlation locally), because the radio luminosities used here were derived based on the observational data only, independent of the SED modeling.

5.4.2. AGN activity

As discussed in Section 5.4.1, AGN activity could explain low q values of SMGs. This is at least true for the two SMGs with lowest q^9 , spectroscopically classified as AGN (Chapman et al., 2005).

In the SEDs of SMGs there are clear signs that some of them host AGNs (though, not necessarily a bolometrically dominant ones). Radio datapoints are higher than model predictions by more than 3σ in 36% (27/76) of SMGs, whereas they are lower than models only for 8% (6/76). This may hint at an AGN contribution in these galaxies. However, 4 out of 5 X-ray identified starbursts (Column 16 of Table A.3) also exhibit radio excess, so we find other explanations of radio excess presented in Section 5.4.1 more reliable.

Another indication of an AGN contribution is that 18% (14/76) of SMGs show a mid-IR power-law AGN feature incompatible with our starburst models (see Figure A.1 and Column 16 of Table A.3). However, rest-frame 2–5 μm excess was also interpreted as a tracer of recent star formation (Mentuch et al., 2009).

Finally, three SMGs¹⁰ have exceptionally high SFR_{UV} ($> 500 M_{\odot} \text{yr}^{-1}$, Column 4 of Table A.3). Strikingly, all of them were fitted with non-starburst models ($M_{\text{burst}} = 0$, Column 9), so modeling is consistent with these high SFRs being continuous (the same is true for three other non-starburst SMGs with high SFR_{IR}). Such a scenario is

⁹ SMMJ131215.27+423900.9, SMMJ141813.54+522923.4

¹⁰ SMMJ123716.01+620323.3, SMMJ131215.27+423900.9, SMMJ131222.35+423814.1

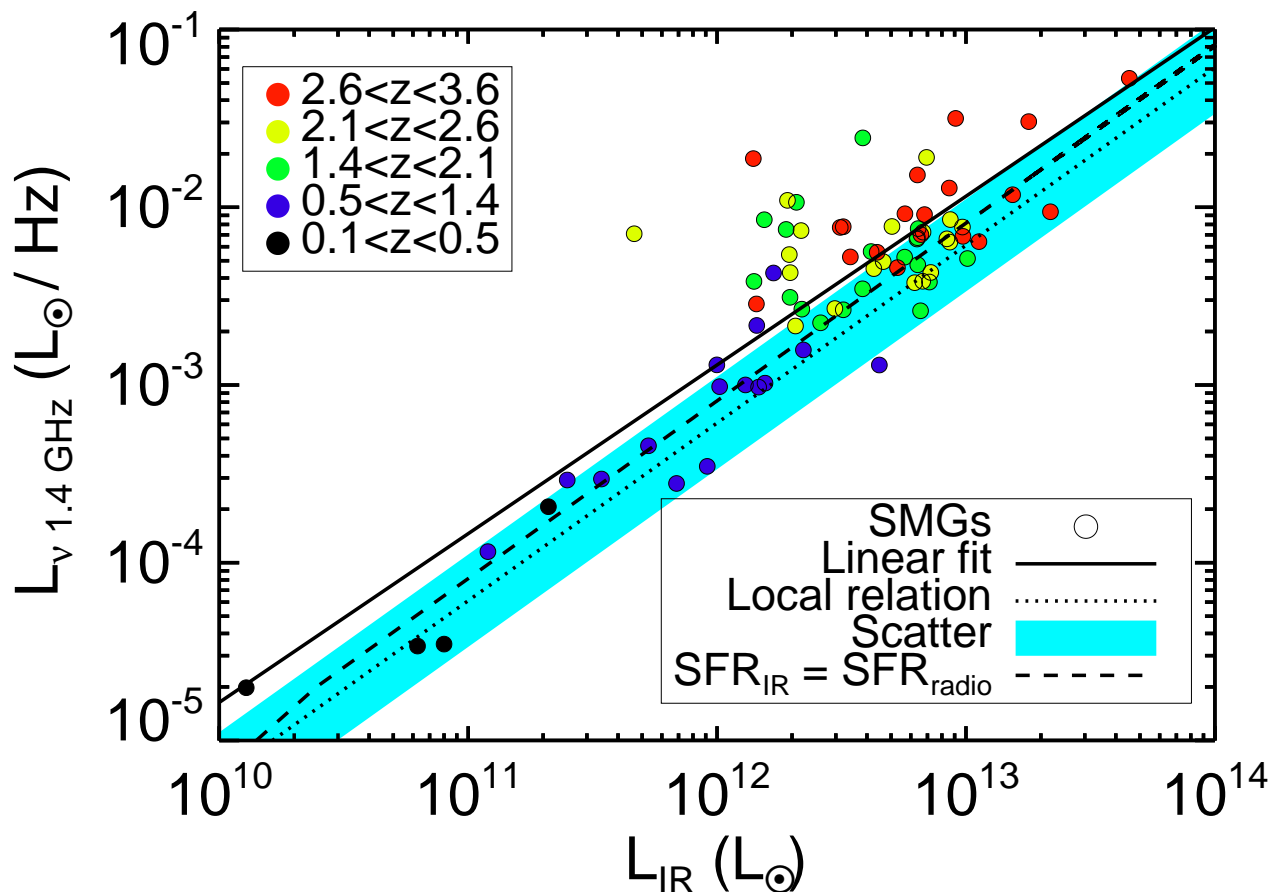


Fig. 5 Radio luminosity density as a function of infrared (8–1000 μm) luminosity of SMGs showing a linear relation, though with a normalization offset from the local relation by a factor of ~ 2.1 towards higher radio luminosities (Section 5.4.1). *Circles*: values for individual SMGs color-coded by redshift. *Solid line*: linear fit to the data (eq. 1). *Dotted line*: the mean local relation (Bell, 2003). *Shaded area*: its scatter. *Dashed line*: the track where SFR_{IR} (Kennicutt, 1998) is equal to $\text{SFR}_{\text{radio}}$ (Bell, 2003). The strong outliers (above the line) at high-luminosity end are probably caused by AGN activity increasing radio luminosities.

unlikely, so this hints at an AGN contribution to the UV/IR emission.

However, the fact that we obtained reasonable SED fits for most of the SMGs using purely star-forming models (Figure A.1) hints at the conclusion that AGN activity is not dominant in our sample.

We investigated the issue of AGN activity further by analysing the average q values of the following subsamples (see also Figure 6): X-ray identified (Alexander et al., 2005) AGNs: 2.32 ± 0.06 and starbursts: 2.12 ± 0.18 ; optically identified AGNs (Chapman et al., 2005): 2.27 ± 0.09 ; and mid-IR identified AGNs (see above): 2.36 ± 0.12 . All subsamples are consistent with the value derived for the entire sample (2.32). Hence, we confirm the finding of Hainline (2008) that even the AGN-classified SMGs follow a linear IR-radio correlation. This means that even if an AGN is present it does not contribute to the emission of an SMG significantly (with the exception of the two $q \sim 1.3$ sources).

This is in line with *i*) the X-ray studies of SMGs indicating that the contribution of AGN activity to their IR emission is only $\sim 8\%$ on average (Alexander et al., 2005); *ii*) mid-IR colors of SMGs indicating that AGNs dominate the emission at these wavelengths only in 13–19% cases (Hainline et al., 2009); *iii*) mid-IR spectroscopy of SMGs

revealing only weak AGN-like continua (Valiante et al., 2007; Pope et al., 2008; Menéndez-Delmestre et al., 2007, 2009; Murphy et al., 2009; Watabe et al., 2009); *iv*) near-IR spectroscopy revealing that starbursts dominate the emission of SMGs (Swinbank et al., 2004). Moreover, de Vries et al. (2007) found that star formation processes (if present) account for at least 75% of the radio luminosities of optically-selected AGNs.

Therefore we conclude that AGNs are present in a significant fraction of SMGs, but their contribution to the IR emission is at most minor.

5.5. Comparison of our results with the literature

For the sample of SMGs discussed in this paper there are previous estimates of some of their properties. In this section we compare them with our results.

Chapman et al. (2005) derived L_{IR} and T_d based only on the 850 μm and 1.4 GHz data. There is no systematic difference between the determinations of T_d (our median of 38.7 K, theirs: 38.3 K). The mean difference between individual datapoints is 4 K ($\sim 10\%$). However, our values for L_{IR} are systematically lower than theirs (the me-

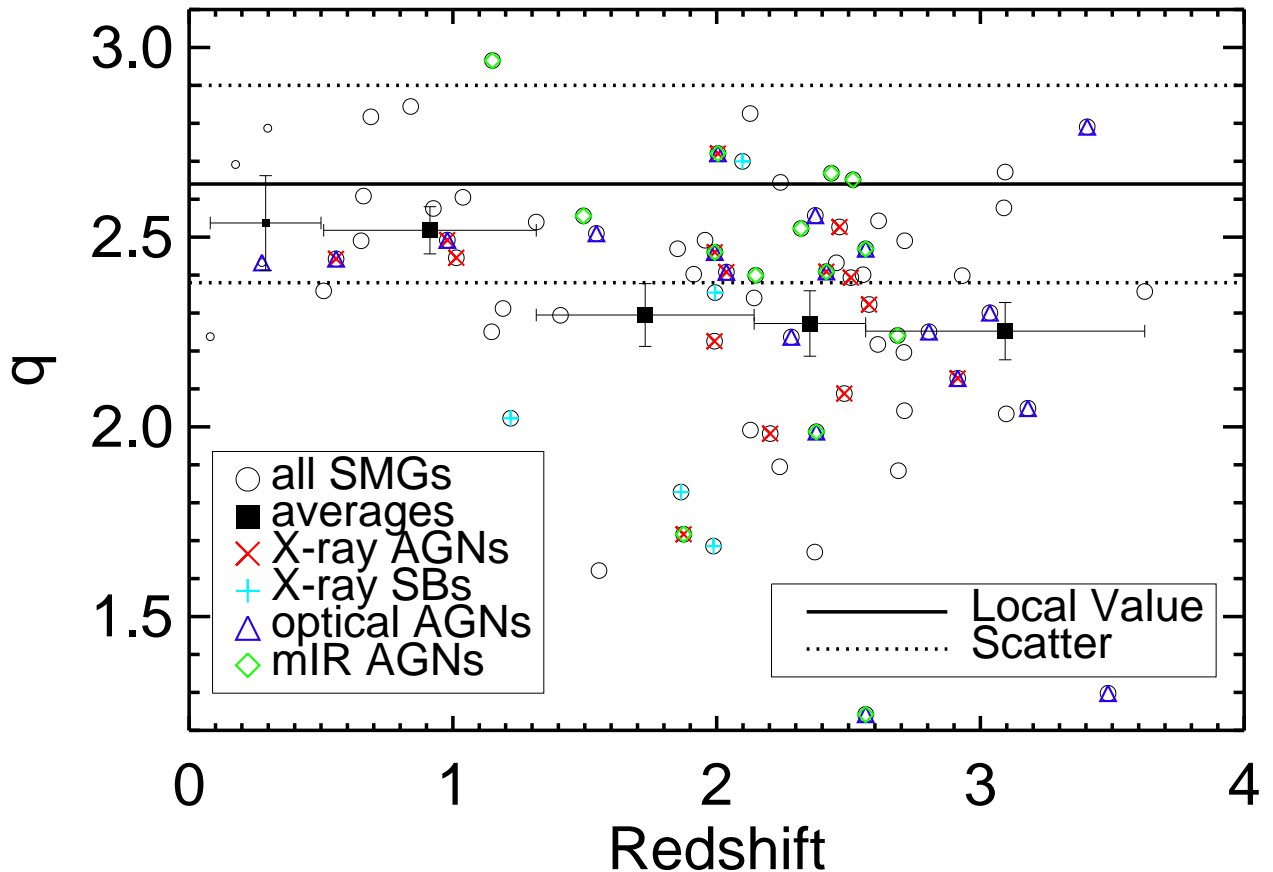


Fig. 6 The ratio of the infrared (8–1000 μm) and radio luminosities q (defined in Section 3.1) as a function of redshift of SMGs. It provides evidence that a linear IR-radio correlation holds for SMGs up to $z \sim 3.6$, though with a normalization offset from the local relation by a factor of ~ 2.1 ($\Delta q \sim -0.32$) towards higher radio luminosities (Section 5.4.1). *Circles*: values for individual SMGs. *Squares*: the mean values (and errors on the mean) in five redshift bins containing equal number of galaxies (Table 1 and Section 3.2). *Small symbols* indicate $z < 0.5$ objects. *Red crosses*: SMGs classified as AGNs based on X-ray emission (Alexander et al., 2005). *Light blue plus signs*: SMGs classified as starbursts based on X-ray emission (Alexander et al., 2005). *Violet triangles*: SMGs classified as AGNs based on optical spectra (Chapman et al., 2005). *Green diamonds*: SMGs classified as AGNs based on a mid-IR power-law (Section 5.4.2). The mean local $q = 2.64$ (Bell, 2003) is shown as a *solid line* with 0.26 scatter (*dotted lines*). The q values for majority of AGN-classified SMGs do not differ from the rest of the SMG population (see Section 5.4.2).

dian ratio of individual datapoints is 1.7). We find our values more reliable since they are based on data spanning a wider wavelength range. Overestimation of L_{IR} when using only 850 μm and 1.4 GHz was also noticed by Kovács et al. (2006) and Pope et al. (2006).

Kovács et al. (2006) investigated a subsample observed at 350 μm . Their median dust mass ($9.04 \log M_{\odot}$) and q value (2.20) are consistent with our estimates (9.01 and 2.35, respectively). The median difference between individual datapoints is $\sim 30\%$ for dust masses and $\sim 13\%$ for q .

The median stellar mass for a subsample of 13 SMGs investigated by Borys et al. (2005, $11.51 \log M_{\odot}$) is close to our value (11.70). However, estimates of Hainline (2008, median $10.82 \log M_{\odot}$) for 64 SMGs are a factor of ~ 5.6 smaller than our values (11.57). Hainline (2008) postulated that the discrepancy between her results and those of Borys et al. (2005) arose from a combination of systematic differences between the applied SED models and a higher AGN contribution in the K -band (used by Borys et al.,

2005) with respect to the H -band. Our estimates are based on all the available photometric data, and so we find the former explanation more likely. In particular, the differences in the applied stellar population models and their ages may explain the discrepancy.

6. Conclusions

We have investigated the UV-to-radio SEDs of 76 SMGs ($S_{850} \gtrsim 3 \text{ mJy}$) with spectroscopic redshifts (0.080–3.623). For the first time the properties of such a significant sample has been derived consistently using all available data. The resulting SFRs (median $713 M_{\odot} \text{ yr}^{-1}$) and stellar masses ($11.57 \log M_{\odot}$) are among the highest in the Universe.

Such high stellar masses, already present at redshifts ~ 2 –3, require that SMGs experienced either at least two starburst episodes, or a merger of several smaller galaxies. Our modeling suggests that only a minor fraction (8%) of their stellar populations was formed during the ongoing starburst episodes. This is supported by the fact that the

SFRs and M_* of SMGs are basically disconnected, i.e. we observe two orders of magnitude spread in SSFRs whereas the range of M_* is relatively narrow: 10^{11} – $10^{12} M_\odot$. We concluded that dust is blown away or destroyed during the evolution of SMGs, since it is not stored in the likely end-products of SMGs, elliptical galaxies.

Indeed, the high stellar masses and the evolution of the SFR and stellar mass densities of SMGs are consistent with a scenario in which SMGs are progenitors of present-day ellipticals.

We found that SMGs contribute significantly to the cosmic SFR, ρ_{SFR} ($\sim 20\%$) and stellar mass, ρ_* (30–50%) densities at $z \sim 2$ –4. If we consider submillimeter sources down to 0.1 mJy the contribution to ρ_{SFR} rises to $\sim 80\%$.

Our analysis suggests that a linear IR-radio correlation holds for SMGs at least up to a redshift of 3.6, but they are ~ 2.1 times brighter at radio wavelengths than what would result from the local correlation.

Acknowledgements. We thank Joanna Baradziej, José María Castro Cerón, Thomas Greve, Brian Lacki, Kim Nilsson, Jesper Sommer-Larsen, Sune Toft, Bärbel Tress and Gunther Tress for discussion and comments; our referee for help with improving this paper; Scott Chapman for information on the survey areas; Jorge Iglesias-Páramo for kindly providing his SED templates; and Fabio Fontanot for kindly providing his model and data on star formation density. We acknowledge use of the extensive *Spitzer* database in the PhD thesis of Laura Hainline.

M. J. M. would like to acknowledge support from The Faculty of Science, University of Copenhagen. The Dark Cosmology Centre is funded by the Danish National Research Foundation. This research has made use of NASA's Astrophysics Data System Bibliographic Services.

References

- Ajiki M., et al., 2003, *AJ*, 126, 2091
 Alexander D.M., Bauer F.E., Chapman S.C., Smail I., Blain A.W., Brandt W.N., Ivison R.J., 2005, *ApJ*, 632, 736
 Alexander D.M., et al., 2008, *AJ*, 135, 1968
 Almaini O., et al., 2003, *MNRAS*, 338, 303
 Appleton P.N., et al., 2004, *ApJS*, 154, 147
 Aravena M., et al., 2010, *ApJ*, 708, L36
 Arnouts S., et al., 2007, *A&A*, 476, 137
 Ashby M.L.N., et al., 2006, *ApJ*, 644, 778
 Austermann J.E., et al., 2009, *MNRAS*, 393, 1573
 Barger A.J., Cowie L.L., Sanders D.B., 1999, *ApJ*, 518, L5
 Barger A.J., Cowie L.L., Richards E.A., 2000, *AJ*, 119, 2092
 Bell E.F., 2003, *ApJ*, 586, 794
 Bell E.F., McIntosh D.H., Katz N., Weinberg M.D., 2003, *ApJS*, 149, 289
 Bell E.F., Zheng X.Z., Papovich C., Borch A., Wolf C., Meisenheimer K., 2007, *ApJ*, 663, 834
 Berciano Alba A., Koopmans L.V.E., Garrett M.A., Wucknitz O., Limousin M., 2010, *A&A*, 509, 54
 Beswick R.J., Muxlow T.W.B., Thrall H., Richards A.M.S., Garrington S.T., 2008, *MNRAS*, 385, 1143
 Blain A.W., 1997, *MNRAS*, 290, 553
 Blain A.W., Longair M.S., 1996, *MNRAS*, 279, 847
 Blain A.W., Kneib J., Ivison R.J., Smail I., 1999, *ApJ*, 512, L87
 Blain A.W., Smail I., Ivison R.J., Kneib J.P., Frayer D.T., 2002, *Phys. Rep.*, 369, 111
 Blain A.W., Chapman S.C., Smail I., Ivison R., 2004, *ApJ*, 611, 52
 Borch A., et al., 2006, *A&A*, 453, 869
 Borys C., Smail I., Chapman S.C., Blain A.W., Alexander D.M., Ivison R.J., 2005, *ApJ*, 635, 853
 Bouwens R., Broadhurst T., Illingworth G., 2003a, *ApJ*, 593, 640
 Bouwens R.J., et al., 2003b, *ApJ*, 595, 589
 Bouwens R.J., et al., 2004, *ApJ*, 606, L25
 Bouwens R.J., Illingworth G.D., Blakeslee J.P., Franx M., 2006, *ApJ*, 653, 53
 Bouwens R.J., Illingworth G.D., Franx M., Ford H., 2007, *ApJ*, 670, 928
 Boyle B.J., Cornwell T.J., Middelberg E., Norris R.P., Appleton P.N., Smail I., 2007, *MNRAS*, 376, 1182
 Brinchmann J., Ellis R.S., 2000, *ApJ*, 536, L77
 Brinchmann J., Charlot S., White S.D.M., Tremonti C., Kauffmann G., Heckman T., Brinkmann J., 2004, *MNRAS*, 351, 1151
 Bundy K., et al., 2006, *ApJ*, 651, 120
 Bunker A.J., Stanway E.R., Ellis R.S., McMahon R.G., 2004, *MNRAS*, 355, 374
 Capak P., et al., 2004, *AJ*, 127, 180
 Capak P., et al., 2008, *ApJ*, 681, L53
 Caputi K.I., McLure R.J., Dunlop J.S., Cirasuolo M., Schael A.M., 2006, *MNRAS*, 366, 609
 Caputi K.I., et al., 2007, *ApJ*, 660, 97
 Castro Cerón J.M., Michałowski M., Hjorth J., Watson D.J., Fynbo J.P.U., Gorosabel J., 2006, *ApJL*, 653, L85
 Castro Cerón J.M., Michałowski M.J., Hjorth J., Malesani D., Gorosabel J., Watson D., Fynbo J.P.U., 2009, *ApJ*, submitted, [arXiv:0803.2235v1](https://arxiv.org/abs/0803.2235v1) [astro-ph]
 Chapman S.C., Richards E.A., Lewis G.F., Wilson G., Barger A.J., 2001, *ApJ*, 548, L147
 Chapman S.C., et al., 2003a, *ApJ*, 585, 57
 Chapman S.C., Windhorst R., Odewahn S., Yan H., Conselice C., 2003b, *ApJ*, 599, 92
 Chapman S.C., Smail I., Windhorst R., Muxlow T., Ivison R.J., 2004, *ApJ*, 611, 732
 Chapman S.C., Blain A.W., Smail I., Ivison R.J., 2005, *ApJ*, 622, 772
 Clements D., et al., 2004, *MNRAS*, 351, 447
 Clements D.L., et al., 2008, *MNRAS*, 387, 247
 Cohen J.G., 2002, *ApJ*, 567, 672
 Cole S., et al., 2001, *MNRAS*, 326, 255
 Condon J.J., 1989, *ApJ*, 338, 13
 Condon J.J., 1992, *ARA&A*, 30, 575
 Condon J.J., Cotton W.D., Broderick J.J., 2002, *AJ*, 124, 675
 Connolly A.J., Szalay A.S., Dickinson M., Subbarao M.U., Brunner R.J., 1997, *ApJ*, 486, L11
 Conselice C.J., Blackburne J.A., Papovich C., 2005, *ApJ*, 620, 564
 Coppin K., et al., 2006, *MNRAS*, 372, 1621
 Coppin K., et al., 2008, *MNRAS*, 384, 1597
 Coppin K.E.K., et al., 2009, *MNRAS*, 395, 1905
 Courty S., Björnsson G., Gudmundsson E.H., 2007, *MNRAS*, 376, 1375
 Cowie L.L., Hu E.M., 1998, *AJ*, 115, 1319
 Cowie L.L., Songaila A., Hu E.M., Cohen J.G., 1996, *AJ*, 112, 839
 Cowie L.L., Songaila A., Barger A.J., 1999, *AJ*, 118, 603
 Cowie L.L., Barger A.J., Kneib J., 2002, *AJ*, 123, 2197
 Daddi E., Cimatti A., Renzini A., 2000, *A&A*, 362, L45
 Daddi E., Dannerbauer H., Krips M., Walter F., Dickinson M., Elbaz D., Morrison G.E., 2009a, *ApJ*, 695, L176
 Daddi E., et al., 2009b, *ApJ*, 694, 1517
 Dahlen T., Mobasher B., Dickinson M., Ferguson H.C., Giavalisco M., Kretchmer C., Ravindranath S., 2007, *ApJ*, 654, 172
 Davé R., Finlator K., Oppenheimer B.D., Fardal M., Katz N., Kereš D., Weinberg D.H., 2009, *MNRAS*, submitted, [arXiv:0909.4078](https://arxiv.org/abs/0909.4078) [astro-ph.CO]
 de Ravel L., et al., 2009, *A&A*, 498, 379
 de Vries W.H., Hodge J.A., Becker R.H., White R.L., Helfand D.J., 2007, *AJ*, 134, 457
 Devlin M.J., et al., 2009, *Nature*, 458, 737
 Dickinson M., Papovich C., Ferguson H.C., Budavári T., 2003, *ApJ*, 587, 25
 Driver S.P., et al., 2006, *MNRAS*, 368, 414
 Driver S.P., Popescu C.C., Tuffs R.J., Liske J., Graham A.W., Allen P.D., de Propriis R., 2007, *MNRAS*, 379, 1022
 Drory N., Bender R., Feulner G., Hopp U., Maraston C., Snigula J., Hill G.J., 2004, *ApJ*, 608, 742
 Drory N., Salvato M., Gabasch A., Bender R., Hopp U., Feulner G., Pannella M., 2005, *ApJ*, 619, L131
 Dunne L., et al., 2009, *MNRAS*, 394, 3
 Dye S., et al., 2008, *MNRAS*, 386, 1107
 Dye S., et al., 2009, *ApJ*, 703, 285
 Eales S., Lilly S., Gear W., Dunne L., Bond J.R., Hammer F., Le Fèvre O., Crampton D., 1999, *ApJ*, 515, 518
 Eales S., et al., 2009, *ApJ*, 707, 1779
 Egami E., et al., 2004, *ApJS*, 154, 130
 Elsner F., Feulner G., Hopp U., 2008, *A&A*, 477, 503
 Erb D.K., Steidel C.C., Shapley A.E., Pettini M., Reddy N.A., Adelberger K.L., 2006, *ApJ*, 646, 107
 Eyles L.P., Bunker A.J., Ellis R.S., Lacy M., Stanway E.R., Stark

- D.P., Chiu K., 2007, *MNRAS*, 374, 910
- Flores H., et al., 1999, *ApJ*, 517, 148
- Fomalont E.B., Kellermann K.I., Cowie L.L., Capak P., Barger A.J., Partridge R.B., Windhorst R.A., Richards E.A., 2006, *ApJS*, 167, 103
- Fontana A., et al., 2003, *ApJ*, 594, L9
- Fontana A., et al., 2004, *A&A*, 424, 23
- Fontana A., et al., 2006, *A&A*, 459, 745
- Franceschini A., et al., 2006, *A&A*, 453, 397
- Frazer D.T., et al., 2004, *ApJS*, 154, 137
- Fujita S.S., et al., 2003a, *AJ*, 125, 13
- Fujita S.S., et al., 2003b, *ApJ*, 586, L115
- Gallego J., Zamorano J., Aragon-Salamanca A., Rego M., 1995, *ApJ*, 455, L1
- Gallego J., García-Dabó C.E., Zamorano J., Aragón-Salamanca A., Rego M., 2002, *ApJ*, 570, L1
- Garn T., Green D.A., Riley J.M., Alexander P., 2009, *MNRAS*, 397, 1101
- Garrett M.A., 2002, *A&A*, 384, L19
- Geach J.E., Smail I., Best P.N., Kurk J., Casali M., Ivison R.J., Coppin K., 2008, *MNRAS*, 388, 1473
- Genzel R., et al., 2008, *ApJ*, 687, 59
- Georgakakis A., Hopkins A.M., Sullivan M., Afonso J., Georgantopoulos I., Mobasher B., Cram L.E., 2003, *MNRAS*, 345, 939
- Giavalisco M., et al., 2004, *ApJ*, 600, L103
- Glazebrook K., Blake C., Economou F., Lilly S., Colless M., 1999, *MNRAS*, 306, 843
- Glazebrook K., et al., 2004, *Nature*, 430, 181
- Greve T.R., Ivison R.J., Bertoldi F., Stevens J.A., Dunlop J.S., Lutz D., Carilli C.L., 2004, *MNRAS*, 354, 779
- Greve T.R., et al., 2005, *MNRAS*, 359, 1165
- Gronwall C., 1999, *AIPC*, 470, 335
- Gronwall C., et al., 2007, *ApJ*, 667, 79
- Gruppioni C., Pozzi F., Zamorani G., Ciliegi P., Lari C., Calabrese E., La Franca F., Matute I., 2003, *MNRAS*, 341, L1
- Gwyn S.D.J., Hartwick F.D.A., 2005, *AJ*, 130, 1337
- Haarsma D.B., Partridge R.B., Windhorst R.A., Richards E.A., 2000, *ApJ*, 544, 641
- Hainline L.J., 2008, *Multi-Wavelength Properties of Submillimeter-Selected Galaxies*, Ph.D. thesis, California Institute of Technology
- Hainline L.J., Blain A.W., Greve T.R., Chapman S.C., Smail I., Ivison R.J., 2006, *ApJ*, 650, 614
- Hainline L.J., Blain A.W., Smail I., Frazer D.T., Chapman S.C., Ivison R.J., Alexander D.M., 2009, *ApJ*, 699, 1610
- Hammer F., et al., 1997, *ApJ*, 481, 49
- Hanish D.J., et al., 2006, *ApJ*, 649, 150
- Helou G., Soifer B.T., Rowan-Robinson M., 1985, *ApJ*, 298, L7
- Hippelein H., et al., 2003, *A&A*, 402, 65
- Hogg D.W., Cohen J.G., Blandford R., Pahre M.A., 1998, *ApJ*, 504, 622
- Holland W.S., et al., 1999, *MNRAS*, 303, 659
- Hopkins A.M., 2004, *ApJ*, 615, 209
- Hopkins A.M., Beacom J.F., 2006, *ApJ*, 651, 142
- Hopkins A.M., Connolly A.J., Szalay A.S., 2000, *AJ*, 120, 2843
- Hu E.M., Cowie L.L., McMahon R.G., 1998, *ApJ*, 502, L99
- Hughes D.H., et al., 1998, *Nature*, 394, 241
- Huyhn M.T., Pope A., Frazer D.T., Scott D., 2007, *ApJ*, 659, 305
- Ibar E., et al., 2008, *MNRAS*, 386, 953
- Iglesias-Páramo J., et al., 2007, *ApJ*, 670, 279
- Ilbert O., et al., 2010, *ApJ*, 709, 644
- Ivison R.J., Dunlop J.S., Smail I., Dey A., Liu M.C., Graham J.R., 2000, *ApJ*, 542, 27
- Ivison R.J., et al., 2002, *MNRAS*, 337, 1
- Ivison R.J., et al., 2004, *ApJS*, 154, 124
- Ivison R.J., et al., 2005, *MNRAS*, 364, 1025
- Ivison R.J., et al., 2009, *MNRAS*, 1794+–
- Iwata I., Ohta K., Tamura N., Ando M., Wada S., Watanabe C., Akiyama M., Aoki K., 2003, *PASJ*, 55, 415
- Iwata I., Ohta K., Tamura N., Akiyama M., Aoki K., Ando M., Kiuchi G., Sawicki M., 2007, *MNRAS*, 376, 1557
- Kennicutt R.C., 1998, *ARA&A*, 36, 189
- Knudsen K.K., Kneib J.P., Egami E., 2008a, In: Chary R.R., Teplitz H.I., Sheth K. (eds.) *Infrared Diagnostics of Galaxy Evolution*, vol. 381 of *Astronomical Society of the Pacific Conference Series*, 372
- Knudsen K.K., van der Werf P.P., Kneib J.P., 2008b, *MNRAS*, 384, 1611
- Knudsen K.K., Kneib J., Richard J., Petitpas G., Egami E., 2010, *ApJ*, 709, 210
- Kochanek C.S., et al., 2001, *ApJ*, 560, 566
- Kodaira K., et al., 2003, *PASJ*, 55, L17
- Kovács A., Chapman S.C., Dowell C.D., Blain A.W., Ivison R.J., Smail I., Phillips T.G., 2006, *ApJ*, 650, 592
- Kudritzki R.P., et al., 2000, *ApJ*, 536, 19
- Lacki B.C., Thompson T.A., 2009, *ApJ*, submitted, [arXiv:0910.0478](https://arxiv.org/abs/0910.0478) [[astro-ph.CO](https://arxiv.org/abs/0910.0478)]
- Lacki B.C., Thompson T.A., Quataert E., 2009, *ApJ*, submitted, [arXiv:0907.4161](https://arxiv.org/abs/0907.4161) [[astro-ph.CO](https://arxiv.org/abs/0907.4161)]
- Laurent G.T., et al., 2006, *ApJ*, 643, 38
- Law D.R., Steidel C.C., Erb D.K., Larkin J.E., Pettini M., Shapley A.E., Wright S.A., 2009, *ApJ*, 697, 2057
- Lilly S.J., Le Fevre O., Hammer F., Crampton D., 1996, *ApJ*, 460, L1
- Lilly S.J., Eales S.A., Gear W.K.P., Hammer F., Le Fevre O., Crampton D., Bond J.R., Dunne L., 1999, *ApJ*, 518, 641
- Ly C., et al., 2009, *ApJ*, 697, 1410
- Machalski J., Godlowski W., 2000, *A&A*, 360, 463
- Madau P., Ferguson H.C., Dickinson M.E., Giavalisco M., Steidel C.C., Fruchter A., 1996, *MNRAS*, 283, 1388
- Madau P., Pozzetti L., Dickinson M., 1998, *ApJ*, 498, 106
- Malhotra S., Rhoads J.E., 2004, *ApJ*, 617, L5
- Mann R.G., et al., 2002, *MNRAS*, 332, 549
- Marchesini D., van Dokkum P.G., Förster Schreiber N.M., Franx M., Labbé I., Wuyts S., 2009, *ApJ*, 701, 1765
- Marleau F.R., Fadda D., Appleton P.N., Noriega-Crespo A., Im M., Clancy D., 2007, *ApJ*, 663, 218
- Massarotti M., Iovino A., Buzzoni A., 2001, *ApJ*, 559, L105
- Mauch T., Sadler E.M., 2007, *MNRAS*, 375, 931
- Menéndez-Delmestre K., et al., 2007, *ApJ*, 655, L65
- Menéndez-Delmestre K., et al., 2009, *ApJ*, 699, 667
- Mentuch E., et al., 2009, *ApJ*, 706, 1020
- Michałowski M.J., Hjorth J., 2007, in *AIP Conf. Ser.* 924, *The Multicolored Landscape of Compact Objects and Their Explosive Origins*, ed. L. A. Antonelli et al. (Melville, NY: AIP), 143
- Michałowski M.J., Hjorth J., Castro Cerón J.M., Watson D., 2008, *ApJ*, 672, 817
- Michałowski M.J., et al., 2009, *ApJ*, 693, 347
- Michałowski M.J., Watson D., Hjorth J., 2010, *ApJ*, accepted [arXiv:1002.2636](https://arxiv.org/abs/1002.2636)
- Miller N.A., Owen F.N., 2001, *AJ*, 121, 1903
- Mobasher B., et al., 2009, *ApJ*, 690, 1074
- Moorwood A.F.M., van der Werf P.P., Cuby J.G., Oliva E., 2000, *A&A*, 362, 9
- Murayama T., et al., 2007, *ApJS*, 172, 523
- Murphy E.J., 2009, *ApJ*, 706, 482
- Murphy E.J., Chary R.R., Alexander D.M., Dickinson M., Magnelli B., Morrison G., Pope A., Teplitz H.I., 2009, *ApJ*, 698, 1380
- Narayanan D., Cox T.J., Hayward C.C., Younger J.D., Hernquist L., 2009, *MNRAS*, 400, 1919
- Narayanan D., Hayward C.C., Cox T.J., Hernquist L., Jonsson P., Younger J.D., Groves B., 2010, *MNRAS*, 401, 1613
- Nilsson K.K., et al., 2007, *A&A*, 471, 71
- Nilsson K.K., Tapken C., Möller P., Freudling W., Fynbo J.P.U., Meisenheimer K., Laursen P., Östlin G., 2009, *A&A*, 498, 13
- Ouchi M., et al., 2003, *ApJ*, 582, 60
- Ouchi M., et al., 2004, *ApJ*, 611, 660
- Ouchi M., et al., 2008, *ApJS*, 176, 301
- Paltani S., et al., 2007, *A&A*, 463, 873
- Palunas P., Teplitz H.I., Francis P.J., Williger G.M., Woodgate B.E., 2004, *ApJ*, 602, 545
- Pascale E., et al., 2009, *ApJ*, 707, 1740
- Pascarelle S.M., Lanzetta K.M., Fernández-Soto A., 1998, *ApJ*, 508, L1
- Perera T.A., et al., 2008, *MNRAS*, 391, 1227
- Pérez-González P.G., Zamorano J., Gallego J., Aragón-Salamanca A., Gil de Paz A., 2003, *ApJ*, 591, 827
- Pérez-González P.G., et al., 2005, *ApJ*, 630, 82
- Pérez-González P.G., et al., 2008, *ApJ*, 675, 234
- Pettini M., Kellogg M., Steidel C.C., Dickinson M., Adelberger K.L., Giavalisco M., 1998, *ApJ*, 508, 539
- Pope A., et al., 2006, *MNRAS*, 370, 1185
- Pope A., et al., 2008, *ApJ*, 675, 1171
- Pozzetti L., et al., 2007, *A&A*, 474, 443
- Pozzi F., et al., 2004, *ApJ*, 609, 122
- Rawat A., Hammer F., Kembhavi A.K., Flores H., 2008, *ApJ*, 681, 1089
- Reddy N.A., Steidel C.C., Fadda D., Yan L., Pettini M., Shapley A.E.,

- Erb D.K., Adelberger K.L., 2006, *ApJ*, 644, 792
- Reddy N.A., Steidel C.C., Pettini M., Adelberger K.L., Shapley A.E., Erb D.K., Dickinson M., 2008, *ApJS*, 175, 48
- Rhoads J.E., et al., 2003, *AJ*, 125, 1006
- Rieke G.H., Alonso-Herrero A., Weiner B.J., Pérez-González P.G., Blaylock M., Donley J.L., Marcillac D., 2009, *ApJ*, 692, 556
- Rudnick G., et al., 2003, *ApJ*, 599, 847
- Rudnick G., et al., 2006, *ApJ*, 650, 624
- Sadler E.M., et al., 2002, *MNRAS*, 329, 227
- Sajina A., et al., 2008, *ApJ*, 683, 659
- Salpeter E.E., 1955, *ApJ*, 121, 161
- Salucci P., Persic M., 1999, *MNRAS*, 309, 923
- Santini P., et al., 2009, *A&A*, 504, 751
- Sawicki M., Thompson D., 2006a, *ApJ*, 642, 653
- Sawicki M., Thompson D., 2006b, *ApJ*, 648, 299
- Sawicki M.J., Lin H., Yee H.K.C., 1997, *AJ*, 113, 1
- Schinnerer E., et al., 2008, *ApJ*, 689, L5
- Scott K.S., et al., 2008, *MNRAS*, 385, 2225
- Scott S.E., et al., 2002, *MNRAS*, 331, 817
- Serjeant S., Gruppioni C., Oliver S., 2002, *MNRAS*, 330, 621
- Serjeant S., et al., 2008, *MNRAS*, 386, 1907
- Seymour N., et al., 2008, *MNRAS*, 386, 1695
- Seymour N., Huynh M., Dwelly T., Symeonidis M., Hopkins A., McHardy I.M., Page M.J., Rieke G., 2009, *MNRAS*, 398, 1573
- Shim H., Im M., Choi P., Yan L., Storrie-Lombardi L., 2007, *ApJ*, 669, 749
- Shimasaku K., Ouchi M., Furusawa H., Yoshida M., Kashikawa N., Okamura S., 2005, *PASJ*, 57, 447
- Shimasaku K., et al., 2006, *PASJ*, 58, 313
- Shioya Y., et al., 2008, *ApJS*, 175, 128
- Silva L., Granato G.L., Bressan A., Danese L., 1998, *ApJ*, 509, 103
- Smail I., Ivison R.J., Blain A.W., Kneib J.P., 2002, *MNRAS*, 331, 495
- Smail I., Chapman S.C., Blain A.W., Ivison R.J., 2004, *ApJ*, 616, 71
- Sobral D., et al., 2009, *MNRAS*, 398, 75
- Somerville R.S., Primack J.R., Faber S.M., 2001, *MNRAS*, 320, 504
- Stanway E.R., Bunker A.J., McMahon R.G., 2003, *MNRAS*, 342, 439
- Stark D.P., Bunker A.J., Ellis R.S., Eyles L.P., Lacy M., 2007, *ApJ*, 659, 84
- Stark D.P., Ellis R.S., Bunker A., Bundy K., Targett T., Benson A., Lacy M., 2009, *ApJ*, 697, 1493
- Steidel C.C., Adelberger K.L., Giavalisco M., Dickinson M., Pettini M., 1999, *ApJ*, 519, 1
- Sullivan M., Treyer M.A., Ellis R.S., Bridges T.J., Milliard B., Donas J., 2000, *MNRAS*, 312, 442
- Swinbank A.M., Smail I., Chapman S.C., Blain A.W., Ivison R.J., Keel W.C., 2004, *ApJ*, 617, 64
- Swinbank A.M., Chapman S.C., Smail I., Lindner C., Borys C., Blain A.W., Ivison R.J., Lewis G.F., 2006, *MNRAS*, 371, 465
- Swinbank A.M., et al., 2008, *MNRAS*, 391, 420
- Tacconi L.J., et al., 2006, *ApJ*, 640, 228
- Tacconi L.J., et al., 2008, *ApJ*, 680, 246
- Takagi T., Hanami H., Arimoto N., 2004, *MNRAS*, 355, 424
- Takata T., Sekiguchi K., Smail I., Chapman S.C., Geach J.E., Swinbank A.M., Blain A., Ivison R.J., 2006, *ApJ*, 651, 713
- Tamura Y., et al., 2009, *Nature*, 459, 61
- Taniguchi Y., et al., 2005, *PASJ*, 57, 165
- Teplitz H.I., Collins N.R., Gardner J.P., Hill R.S., Rhodes J., 2003, *ApJ*, 589, 704
- Thompson R.I., Eisenstein D., Fan X., Dickinson M., Illingworth G., Kennicutt R.C. Jr., 2006, *ApJ*, 647, 787
- Trentham N., Blain A.W., Goldader J., 1999, *MNRAS*, 305, 61
- Tresse L., Maddox S.J., 1998, *ApJ*, 495, 691
- Tresse L., Maddox S.J., Le Fèvre O., Cuby J.G., 2002, *MNRAS*, 337, 369
- Treyer M.A., Ellis R.S., Milliard B., Donas J., Bridges T.J., 1998, *MNRAS*, 300, 303
- Valiante E., Lutz D., Sturm E., Genzel R., Tacconi L.J., Lehnert M.D., Baker A.J., 2007, *ApJ*, 660, 1060
- van Breukelen C., Jarvis M.J., Venemans B.P., 2005, *MNRAS*, 359, 895
- van de Ven G., van Dokkum P.G., Franx M., 2003, *MNRAS*, 344, 924
- van Dokkum P.G., Franx M., 2001, *ApJ*, 553, 90
- Villar V., Gallego J., Pérez-González P.G., Pascual S., Noeske K., Koo D.C., Barro G., Zamorano J., 2008, *ApJ*, 677, 169
- Vlahakis C., Eales S., Dunne L., 2007, *MNRAS*, 379, 1042
- Wadadekar Y., Casertano S., de Mello D., 2006, *AJ*, 132, 1023
- Wall J.V., Pope A., Scott D., 2008, *MNRAS*, 383, 435
- Wang W., Cowie L.L., Barger A.J., 2006, *ApJ*, 647, 74
- Wang W.H., Cowie L.L., Barger A.J., 2004, *ApJ*, 613, 655
- Wang W.H., Barger A.J., Cowie L.L., 2009, *ApJ*, 690, 319
- Watabe Y., Risaliti G., Salvati M., Nardini E., Sani E., Marconi A., 2009, *MNRAS*, 396, L1
- Webb T.M., et al., 2003a, *ApJ*, 587, 41
- Webb T.M.A., Lilly S.J., Clements D.L., Eales S., Yun M., Brodwin M., Dunne L., Gear W.K., 2003b, *ApJ*, 597, 680
- Weiß A., Ivison R.J., Downes D., Walter F., Cirasuolo M., Menten K.M., 2009a, *ApJ*, 705, L45
- Weiß A., et al., 2009b, *ApJ*, 707, 1201
- Wilson G., Cowie L.L., Barger A.J., Burke D.J., 2002, *AJ*, 124, 1258
- Wyder T.K., et al., 2005, *ApJ*, 619, L15
- Yan H., Dickinson M., Giavalisco M., Stern D., Eisenhardt P.R.M., Ferguson H.C., 2006, *ApJ*, 651, 24
- Yan L., McCarthy P.J., Freudling W., Teplitz H.I., Malumuth E.M., Weymann R.J., Malkan M.A., 1999, *ApJ*, 519, L47
- Yang M., Greve T.R., Dowell C.D., Borys C., 2007, *ApJ*, 660, 1198
- Yoshida M., et al., 2006, *ApJ*, 653, 988
- Younger J.D., et al., 2007, *ApJ*, 671, 1531
- Younger J.D., et al., 2008, *ApJ*, 688, 59
- Younger J.D., et al., 2009a, *ApJ*, 704, 803
- Younger J.D., et al., 2009b, *MNRAS*, 394, 1685
- Yun M.S., Reddy N.A., Condon J.J., 2001, *ApJ*, 554, 803
- Zheng X.Z., Bell E.F., Papovich C., Wolf C., Meisenheimer K., Rix H.W., Rieke G.H., Somerville R., 2007, *ApJ*, 661, L41

Appendix A: Long tables and figures

Table A.1 Photometry detections of SMGs

SMG	z	λ_{obs} (μm)	flux (μJy)	error (μJy)	Reference
SMMJ030226.17+000624.5	0.080	0.365	33.419	0.306	Clements et al. (2004)
SMMJ030226.17+000624.5	0.080	0.428	83.176	7.319	Chapman et al. (2005)
SMMJ030226.17+000624.5	0.080	0.440	83.946	0.232	Clements et al. (2004)
SMMJ030226.17+000624.5	0.080	0.550	181.970	0.335	Clements et al. (2004)
SMMJ030226.17+000624.5	0.080	0.656	275.423	24.234	Chapman et al. (2005)

Note. — The second reference in the first entry for each SMG indicates that there exists a mid-IR Spitzer/IRS spectrum of this object (Valiante et al., 2007; Pope et al., 2008; Menéndez-Delmestre et al., 2007, 2009). This table is available in its entirety in a machine-readable form in the electronic edition of the Journal. A portion is shown here for guidance regarding its form and content.

References. — Ivison et al. (2002, 2005); Chapman et al. (2003b, 2005); Capak et al. (2004); Clements et al. (2004); Egami et al. (2004); Greve et al. (2004); Smail et al. (2004); Fomalont et al. (2006); Kovács et al. (2006); Laurent et al. (2006); Tacconi et al. (2006); Pope et al. (2006); Huynh et al. (2007); Hainline (2008)

Table A.2 Photometry upper limits of SMGs

SMG	z	λ_{obs} (μm)	flux (μJy)	error (μJy)	Reference
SMMJ030227.73+000653.5	1.408	70.000	13600.000	0.000	Hainline (2008)
SMMJ030231.81+001031.3	1.316	0.365	0.059	0.000	Clements et al. (2004)
SMMJ030231.81+001031.3	1.316	0.428	0.100	0.000	Chapman et al. (2005)
SMMJ030231.81+001031.3	1.316	0.440	0.102	0.000	Clements et al. (2004)
SMMJ030231.81+001031.3	1.316	0.656	0.331	0.000	Chapman et al. (2005)

Note. — When the error is equal to zero, the flux column denotes 3σ upper limit. Otherwise — formal flux at the position of an SMG. This table is available in its entirety in a machine-readable form in the electronic edition of the Journal. A portion is shown here for guidance regarding its form and content.

References. — Ivison et al. (2002, 2005); Chapman et al. (2003b, 2005); Capak et al. (2004); Clements et al. (2004); Egami et al. (2004); Greve et al. (2004); Smail et al. (2004); Fomalont et al. (2006); Kovács et al. (2006); Laurent et al. (2006); Tacconi et al. (2006); Pope et al. (2006); Huynh et al. (2007); Hainline (2008)

Table A.3. Properties of SMGs derived from the SED modeling

SMG (1)	z (2)	SFR ($M_{\odot} \text{ yr}^{-1}$)				SSFR (Gyr^{-1}) (7)	$\log M_*$ (M_{\odot}) (8)	M_{burst}/M_* (%) (9)	M_*/L_K (M_{\odot}/L_{\odot}) (10)	$\log M_d$ (M_{\odot}) (11)	$\log L_{\text{IR}}$ (L_{\odot}) (12)	T_d (K) (13)	A_V (mag) (14)	q (15)	AGN? (16)
		SED (3)	UV (4)	IR (5)	radio (6)										
SMMJ030227.73+000653.5	1.408	825	7.91	713	1190	4.81	11.17	25.5	0.42	8.54	12.62	52.6	1.81	2.29	rad
SMMJ030231.81+001031.3	1.316	433	0.68	224	211	7.81	10.46	71.1	1.36	9.10	12.11	25.6	4.38	2.54	...
SMMJ030236.15+000817.1	2.435	91	4.18	1152	810	3.33	11.54	1.1	0.55	8.62	12.83	41.3	0.27	2.67	mIR,rad
SMMJ105151.69+572636.0	1.147	134	0.30	248	457	0.92	11.43	1.5	0.65	8.97	12.16	34.4	4.00	2.25	rad
SMMJ105155.47+572312.7	2.686	837	12.95	589	1110	1.91	11.49	12.5	0.66	8.90	12.54	38.7	2.29	2.24	mIR
SMMJ105158.02+571800.2	2.239	314	16.77	373	1561	0.44	11.93	0.6	0.60	9.15	12.34	33.2	1.12	1.89	rad
SMMJ105200.22+572420.2	0.689	163	0.26	118	59	0.74	11.20	4.5	1.56	8.72	11.84	33.2	2.58	2.82	...
SMMJ105201.25+572445.7	2.148	935	2.58	798	1044	3.40	11.37	18.1	0.95	9.01	12.67	45.1	2.91	2.40	mIR
SMMJ105207.49+571904.0	2.689	2195	3.81	1559	6679	1.93	11.91	12.5	1.18	8.80	12.96	45.1	2.85	1.88	rad
SMMJ105225.79+571906.4	2.372	217	18.89	329	2310	0.75	11.64	0.0	0.49	8.96	12.28	33.2	1.16	1.67	rad
SMMJ105227.58+572512.4	2.142	410	4.73	376	564	0.57	11.82	1.9	0.78	8.79	12.34	38.7	1.71	2.34	...
SMMJ105227.77+572218.2	1.956	515	1.55	447	473	0.89	11.70	4.5	1.16	9.01	12.42	33.2	2.17	2.49	...
SMMJ105230.73+572209.5	2.611	1255	45.92	975	1942	0.72	12.13	3.8	0.68	9.18	12.75	38.7	1.51	2.22	...
SMMJ105238.19+571651.1	1.852	919	21.87	659	734	4.54	11.16	28.8	0.37	8.85	12.58	38.7	2.13	2.47	...
SMMJ105238.30+572435.8	3.036	1558	7.40	1169	1921	0.69	12.23	3.9	0.85	9.04	12.83	45.1	1.86	2.30	spec
SMMJ123549.44+621536.8	2.203	237	29.23	335	1144	0.70	11.68	0.0	0.51	9.18	12.29	33.2	1.11	1.98	X,rad
SMMJ123553.26+621337.7	2.098	1460	6.05	1223	802	5.73	11.33	31.8	0.42	8.85	12.85	52.6	2.99	2.70	SB
SMMJ123555.14+620901.7	1.875	332	11.94	358	2252	0.61	11.76	1.0	0.61	8.98	12.32	33.2	1.41	1.72	X,mIR,rad
SMMJ123600.10+620253.5	2.710	3733	6.49	3066	6407	8.92	11.54	51.6	0.29	8.52	13.25	71.5	3.64	2.20	rad
SMMJ123600.15+621047.2	1.994	1449	3.04	1102	1602	2.53	11.64	15.2	0.89	9.03	12.81	38.7	2.80	2.35	SB,rad
SMMJ123606.72+621550.7	2.416	448	30.23	354	454	1.27	11.45	6.9	0.65	8.92	12.32	33.2	1.15	2.41	X,spec,mIR
SMMJ123606.85+621021.4	2.509	1291	12.59	1153	1531	1.17	11.99	5.6	0.79	9.34	12.83	33.2	1.58	2.39	X,rad
SMMJ123616.15+621513.7	2.578	968	2.91	754	1179	0.80	11.97	4.5	1.12	9.04	12.64	33.2	2.17	2.32	X
SMMJ123618.33+621550.5	1.865	339	2.20	325	1585	0.66	11.70	2.4	1.10	9.25	12.28	28.5	2.33	1.83	SB,rad
SMMJ123621.27+621708.4	1.988	330	5.65	266	1797	0.32	11.91	1.5	1.30	9.43	12.19	24.4	1.92	1.69	SB,rad
SMMJ123622.65+621629.7	2.466	1981	6.78	1438	1403	1.72	11.92	10.8	0.90	8.90	12.92	45.1	2.40	2.53	X
SMMJ123629.13+621045.8	1.013	202	0.69	176	207	0.35	11.70	1.5	1.53	9.07	12.01	24.4	2.13	2.45	X
SMMJ123632.61+620800.1	1.993	1067	17.30	973	1107	4.52	11.33	22.7	0.45	8.45	12.75	71.5	1.70	2.46	X,spec,mIR,rad
SMMJ123634.51+621241.0	1.219	309	4.49	289	901	0.64	11.66	2.4	1.06	8.93	12.23	28.5	2.16	2.02	SB,rad
SMMJ123635.59+621424.1	2.005	1921	14.81	1740	1087	7.23	11.38	37.1	0.25	8.45	13.01	71.5	2.31	2.72	X,spec,mIR
SMMJ123636.75+621156.1	0.557	11	0.94	21	24	0.69	10.47	0.8	0.67	9.36	11.08	15.2	1.04	2.44	X,spec
SMMJ123707.21+621408.1	2.484	361	4.01	338	905	0.38	11.95	1.3	0.92	8.95	12.29	33.2	1.65	2.09	X,rad
SMMJ123711.98+621325.7	1.992	371	2.50	337	658	1.72	11.29	8.0	0.61	8.64	12.29	45.1	2.30	2.23	X,rad
SMMJ123712.05+621212.3	2.914	150	4.96	247	604	0.20	12.10	0.0	1.32	9.53	12.16	24.4	1.91	2.13	X,spec,rad
SMMJ123716.01+620323.3	2.037	879	567.07	1091	1399	1.28	11.93	0.0	0.31	8.74	12.80	45.1	0.18	2.41	X,spec
SMMJ123721.87+621035.3	0.979	76	2.44	91	96	0.33	11.44	0.6	0.80	9.77	11.72	16.9	1.12	2.49	X,spec
SMMJ131201.17+424208.1	3.405	4375	37.82	3748	1992	16.26	11.36	88.3	0.18	8.14	13.34	113.3	3.08	2.79	spec
SMMJ131208.82+424129.1	1.544	787	3.75	551	560	1.75	11.50	10.9	0.74	8.70	12.51	45.1	1.99	2.51	spec
SMMJ131212.69+424422.5	2.805	2095	2.18	1470	2710	2.22	11.82	14.4	1.29	8.89	12.93	38.7	3.44	2.25	spec,rad
SMMJ131215.27+423900.9	2.565	2361	3387.93	80	1498	0.04	12.32	0.0	0.32	9.90	11.67	15.4	0.00	1.24	spec,mIR
SMMJ131222.35+423814.1	2.565	600	512.57	510	569	0.88	11.76	0.0	0.31	8.75	12.47	33.2	0.10	2.47	spec,mIR
SMMJ131225.20+424344.5	1.038	238	8.94	252	205	2.26	11.05	7.2	0.36	8.42	12.17	38.7	1.46	2.60	...
SMMJ131225.73+423941.4	1.554	742	5.47	661	5188	3.94	11.22	19.1	0.59	8.62	12.59	45.1	2.14	1.62	rad
SMMJ131228.30+424454.8	2.931	1572	16.32	1131	1482	2.43	11.67	15.3	0.61	8.30	12.82	61.3	1.75	2.40	...
SMMJ131231.07+424609.0	2.713	1212	1.42	910	966	5.13	11.25	31.8	0.66	8.70	12.72	45.1	3.95	2.49	...
SMMJ131232.31+423949.5	2.320	2457	8.41	1660	1635	1.60	12.02	10.8	0.87	8.47	12.99	61.3	2.40	2.52	mIR
SMMJ131239.14+424155.7	2.242	1271	3.75	1068	795	3.32	11.51	17.9	0.80	9.01	12.79	38.7	2.87	2.64	...
SMMJ141741.81+522823.0	1.150	948	13.50	770	274	0.75	12.01	3.8	0.72	8.48	12.65	45.1	1.28	2.97	mIR
SMMJ141742.04+523025.7	0.661	403	11.08	267	216	2.02	11.12	13.8	0.40	8.23	11.19	45.1	1.74	2.61	...
SMMJ141750.50+523101.0	2.128	343	5.31	241	808	1.91	11.10	12.5	0.66	8.58	12.15	38.7	2.29	1.99	...
SMMJ141800.40+512820.3	1.913	1999	17.45	1095	1424	0.39	12.44	3.3	0.80	8.61	12.80	52.6	0.89	2.40	...
SMMJ141802.87+523011.1	2.127	1325	10.95	1127	552	11.82	10.98	63.5	0.74	8.34	12.82	61.3	2.87	2.83	...
SMMJ141809.00+522803.8	2.712	1213	6.24	551	1641	0.33	12.23	3.3	0.83	8.64	12.51	45.1	1.09	2.04	...
SMMJ141813.54+522923.4	3.484	243	6.65	240	3967	1.16	11.31	4.2	0.60	8.86	12.15	33.2	1.35	1.30	spec,rad
SMMJ163627.94+405811.2	3.180	1332	18.32	1095	3210	6.32	11.24	34.0	0.65	8.82	12.80	45.1	2.41	2.05	spec
SMMJ163631.47+405546.9	2.283	1325	10.28	865	1646	1.77	11.69	12.5	0.96	8.94	12.70	38.7	2.62	2.24	spec
SMMJ163639.01+405635.9	1.495	250	7.51	1101	1002	6.49	11.23	4.8	0.53	8.94	12.81	32.7	1.46	2.56	mIR,rad
SMMJ163650.43+405734.5	2.378	1147	73.43	1191	4030	3.24	11.57	10.1	0.33	8.93	12.84	45.1	1.12	1.99	spec,mIR,rad
SMMJ163658.19+410523.8	2.454	1769	4.97	1485	1801	2.55	11.77	13.8	0.80	9.04	12.94	45.1	2.45	2.43	...

Table A.3. continued.

SMG (1)	z (2)	SFR ($M_{\odot} \text{ yr}^{-1}$)				SSFR (Gyr^{-1}) (7)	$\log M_*$ (M_{\odot}) (8)	M_{burst}/M_* (%) (9)	M_*/L_K (M_{\odot}/L_{\odot}) (10)	$\log M_d$ (M_{\odot}) (11)	$\log L_{\text{IR}}$ (L_{\odot}) (12)	T_d (K) (13)	A_V (mag) (14)	q (15)	AGN? (16)
		SED (3)	UV (4)	IR (5)	radio (6)										
SMMJ163658.78+405728.1	1.190	129	8.41	171	274	0.56	11.49	0.9	0.59	9.13	11.10	24.4	1.14	2.31	...
SMMJ163704.34+410530.3	0.840	205	2.50	157	74	2.22	10.85	13.1	0.92	9.13	11.96	33.2	2.43	2.84	...
SMMJ163706.51+405313.8	2.374	2020	9.63	1478	1344	1.83	11.91	10.9	0.76	9.06	12.94	45.1	1.99	2.56	spec
SMMJ221724.69+001242.1	0.510	154	14.71	43	62	0.21	11.31	3.4	0.63	9.36	11.40	15.9	0.69	2.36	...
SMMJ221725.97+001238.9	3.094	2499	2.29	1935	1353	2.10	11.96	12.5	1.58	9.38	13.05	38.7	3.27	2.67	...
SMMJ221733.02+000906.0	0.926	447	0.72	381	333	0.88	11.64	4.5	1.56	9.16	12.35	33.2	2.58	2.58	...
SMMJ221733.12+001120.2	0.652	31	2.77	59	62	0.28	11.33	4.7	1.79	9.13	11.54	21.8	1.27	2.49	rad
SMMJ221733.91+001352.1	2.555	875	17.73	731	954	0.78	11.97	3.8	0.79	9.01	12.63	38.7	1.69	2.40	...
SMMJ221735.15+001537.2	3.098	594	8.51	536	1627	2.28	11.37	10.0	0.68	8.94	12.49	38.7	1.93	2.03	...
SMMJ221735.84+001558.9	3.089	1969	7.43	1668	1450	6.49	11.41	35.0	0.30	8.35	12.99	71.5	2.98	2.58	...
SMMJ221737.39+001025.1	2.614	2991	13.32	2641	2484	7.05	11.57	37.1	0.29	8.47	13.19	71.5	2.70	2.54	...
SMMJ221804.42+002154.4	2.517	1474	15.50	1239	908	6.30	11.29	33.5	0.55	8.85	12.86	52.6	2.11	2.65	mIR
SMMJ221806.77+001245.7	3.623	8825	29.59	7774	11225	20.81	11.57	109.9	0.23	8.25	13.66	113.3	3.76	2.36	rad
SMMJ030226.17+000624.5	0.080	3	0.06	2	4	0.07	10.53	0.4	1.08	8.28	10.11	11.4	0.33	2.24	rad
SMMJ030238.62+001106.3	0.276	14	0.04	36	44	59.74	8.78	113.3	0.36	8.32	11.32	25.5	4.22	2.43	spec,rad
SMMJ030244.82+000632.3	0.176	6	0.59	11	7	0.37	10.46	0.0	0.76	8.22	10.80	20.1	1.44	2.69	...
SMMJ123651.76+621221.3	0.298	6	0.12	14	7	1.02	10.13	0.9	0.98	8.91	10.90	13.3	1.93	2.79	...
mean	2.002	1065	68.35	873	1429	3.51	11.71	15.6	0.75	9.02	12.71	40.1	2.03	2.34	...
median	2.148	825	6.78	659	1087	1.72	11.54	7.2	0.68	8.91	12.58	38.7	1.99	2.40	...
std dev	0.851	1271	395.38	1066	1731	7.44	0.55	23.2	0.36	0.36	0.60	18.3	0.95	0.34	...
min	0.080	3	0.04	2	4	0.04	8.78	0.0	0.18	8.14	10.11	11.4	0.00	1.24	...
max	3.623	8825	3387.93	7774	11225	59.74	12.44	113.3	1.79	9.90	13.66	113.3	4.38	2.97	...

Note. — Column (1): SMG name. Column (2): redshift (Chapman et al., 2005). Column (3): total star formation rate (SFR) for 0.15 – 120 M_{\odot} stars averaged over the last 50 Myr derived from the SED model. Column (4): SFR from UV emission interpolated from the SED template (using Kennicutt, 1998). Column (5): SFR from IR emission (Column 12) used in all analysis throughout the paper (using Kennicutt, 1998). Column (6): SFR from radio emission derived directly from the radio data (using Bell, 2003). Column (7): specific SFR $\equiv \text{SFR}_{\text{IR}}/M_*$. Column (8): stellar mass. Column (9): Ratio of the mass of gas converted to star during the recent starburst episode to the total stellar mass. There are values greater than 100%, because the starburst episode is ongoing; 0% means that non-starburst template was adopted. Column (10): stellar mass to light ratio (luminosity at rest-frame K was interpolated using the best SED model). Column (11): dust mass. Column (12): total 8–1000 μm infrared luminosity. Column (13): dust temperature. Column (14): Average extinction $A_V = 2.5 \log(V\text{-band starlight unextinguished} / V\text{-band starlight observed})$. Column (15): FIR-radio correlation parameter (Section 5.4.1). Column (16): AGN flag — X: X-ray identified AGN; SB: X-ray identified starburst (Alexander et al., 2005); spec: spectroscopically identified AGN or QSO (Chapman et al., 2005); mIR: mid-IR identified AGN (Section 5.4.2); rad: radio datapoint is more than 3σ above the starburst model (Section 5.4.2). The horizontal line divides the $z > 0.5$ and $z < 0.5$ samples. This table is available in a machine-readable form in the electronic edition of the Journal.

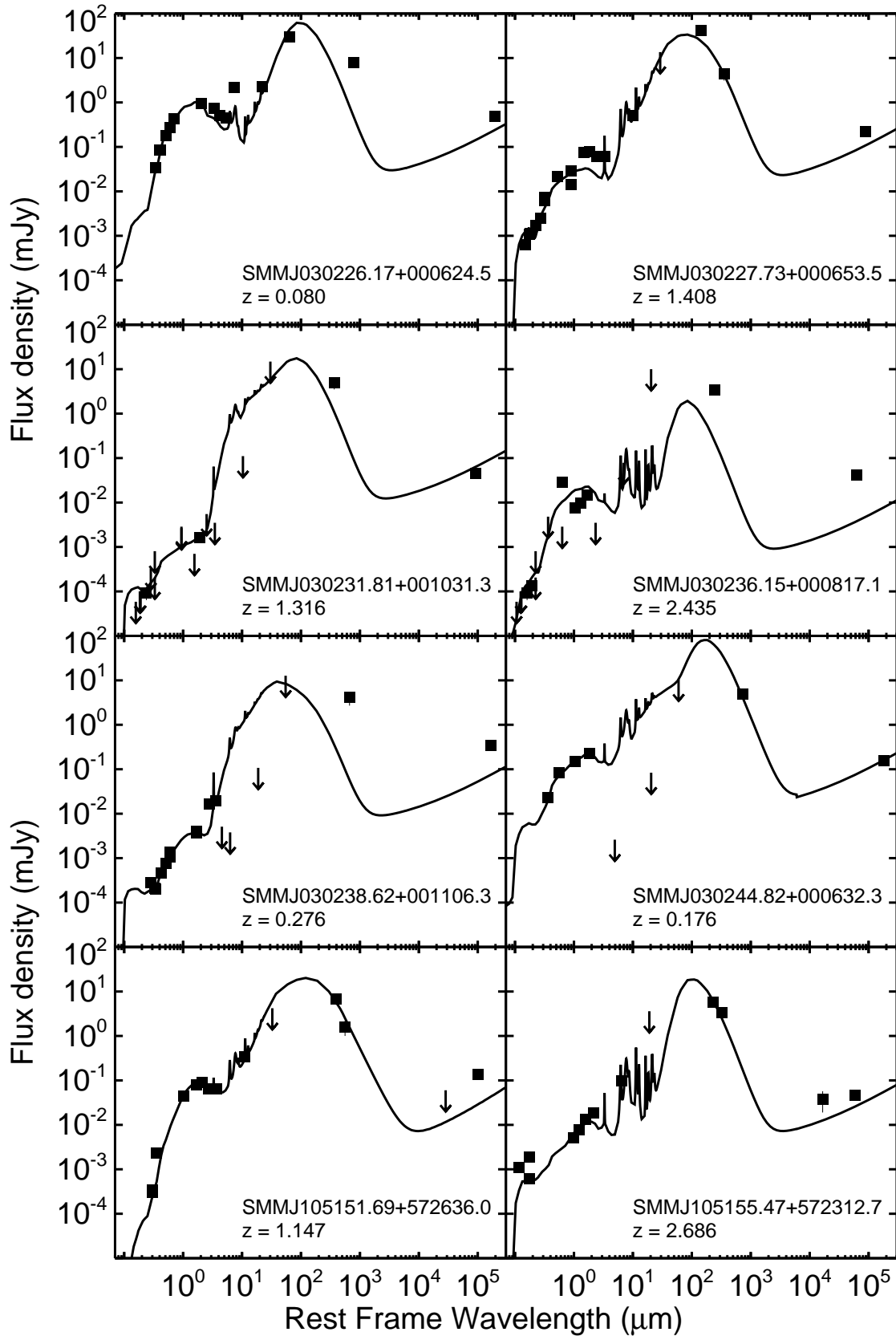


Fig. A.1 Spectral energy distributions (SEDs) of SMGs. *Solid lines*: the best GRASIL fits. *Dashed lines*: SEDs of GRB hosts (Michałowski et al., 2008) shown for comparison. *Squares*: detections with errors, in most cases, smaller than the size of the symbols. *Arrows*: 3σ upper limit (values marked at the base). In the cases where our fits strongly underpredict the observed data at $850\ \mu\text{m}$, we adopted L_{IR} and T_d of Chapman et al. (2005).

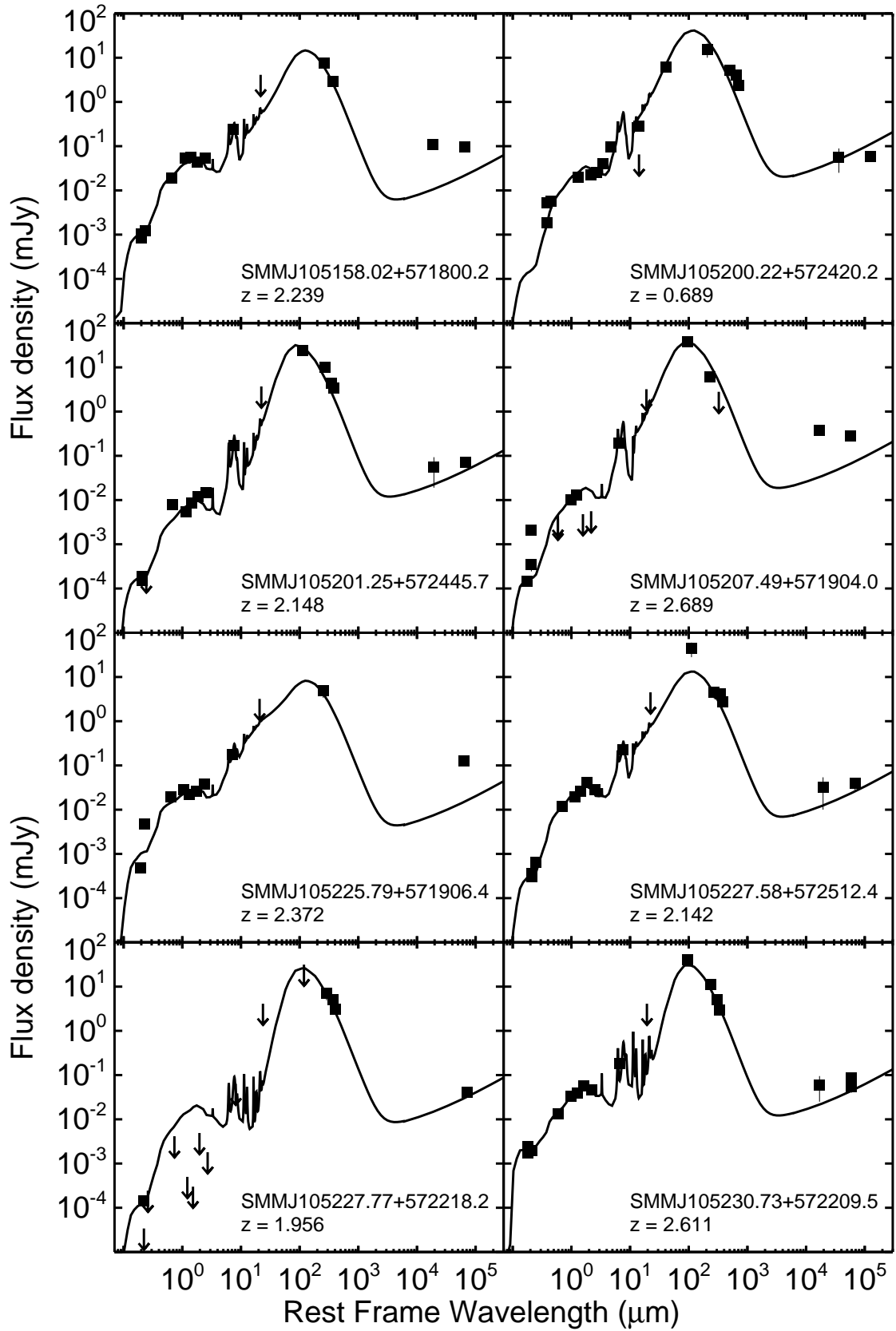


Fig. A.1 (continued).

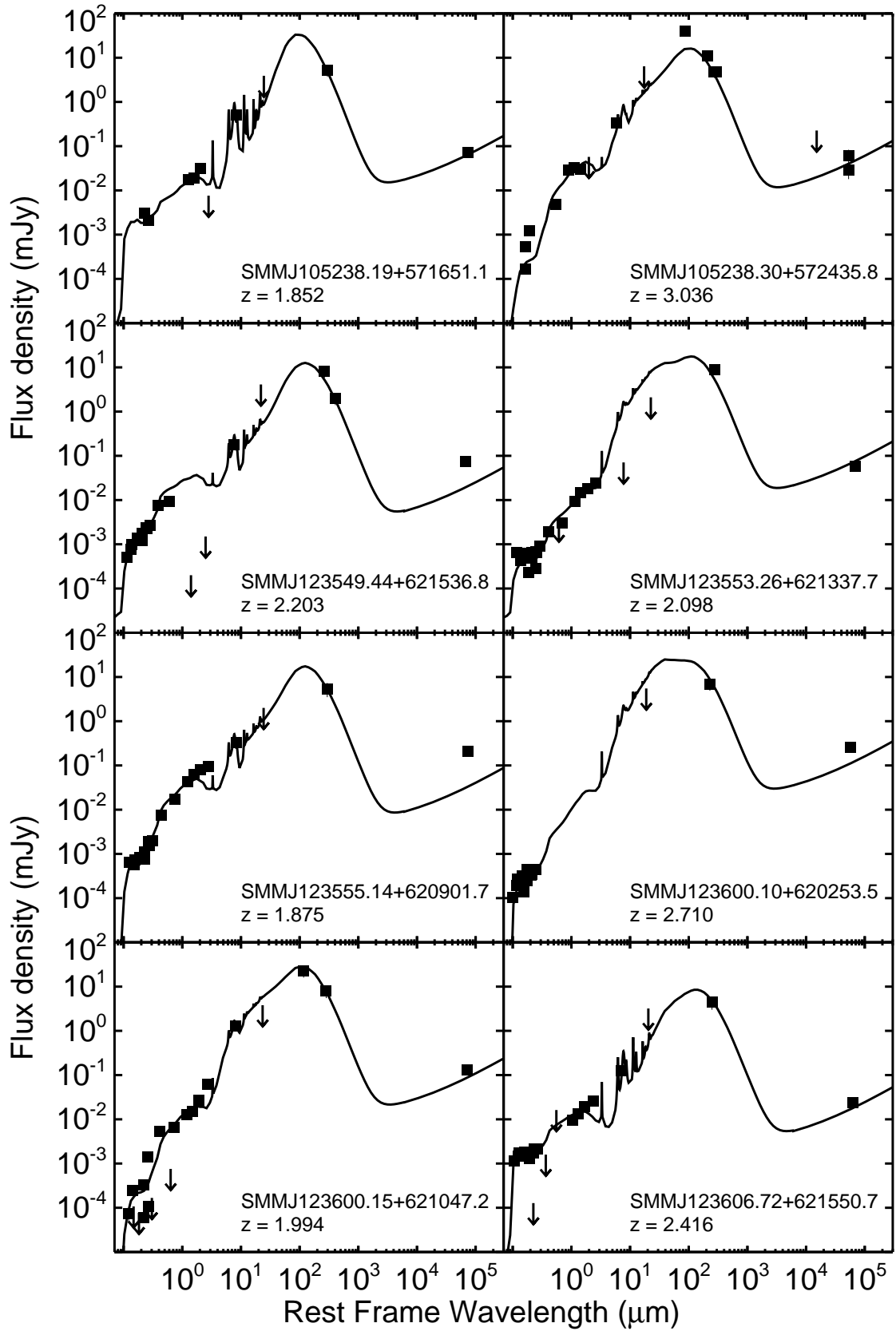


Fig. A.1 (continued).

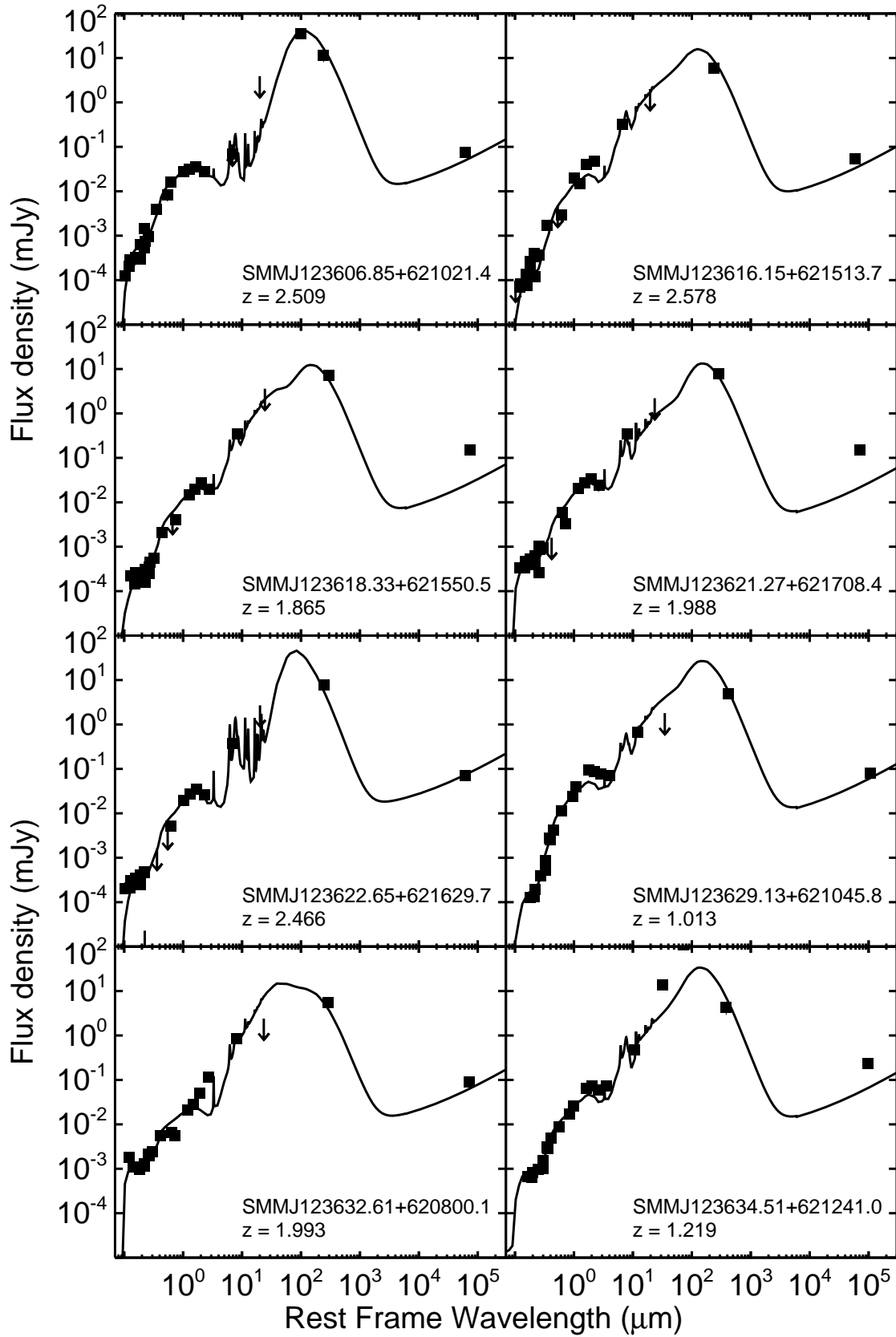


Fig. A.1 (continued).

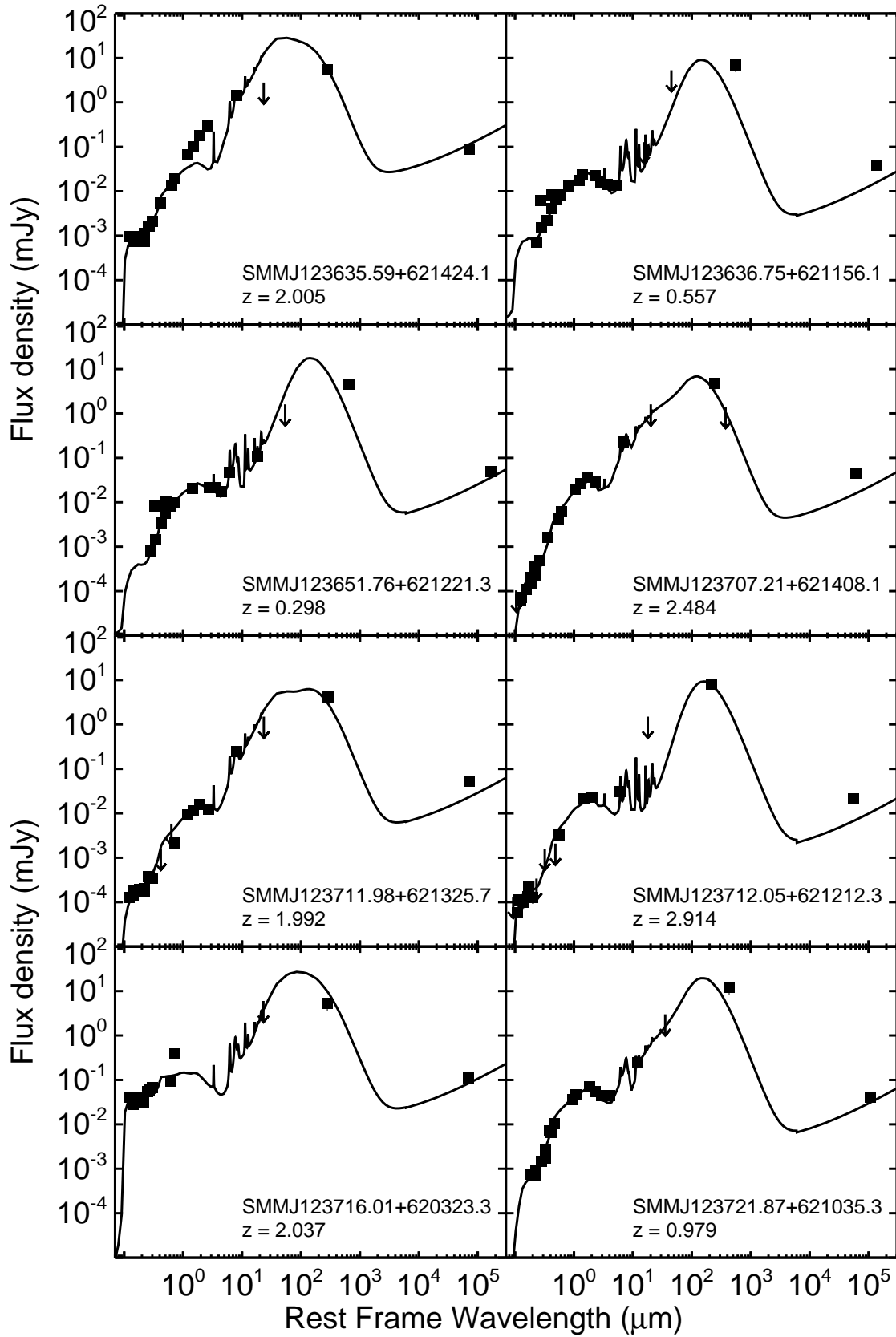


Fig. A.1 (continued).

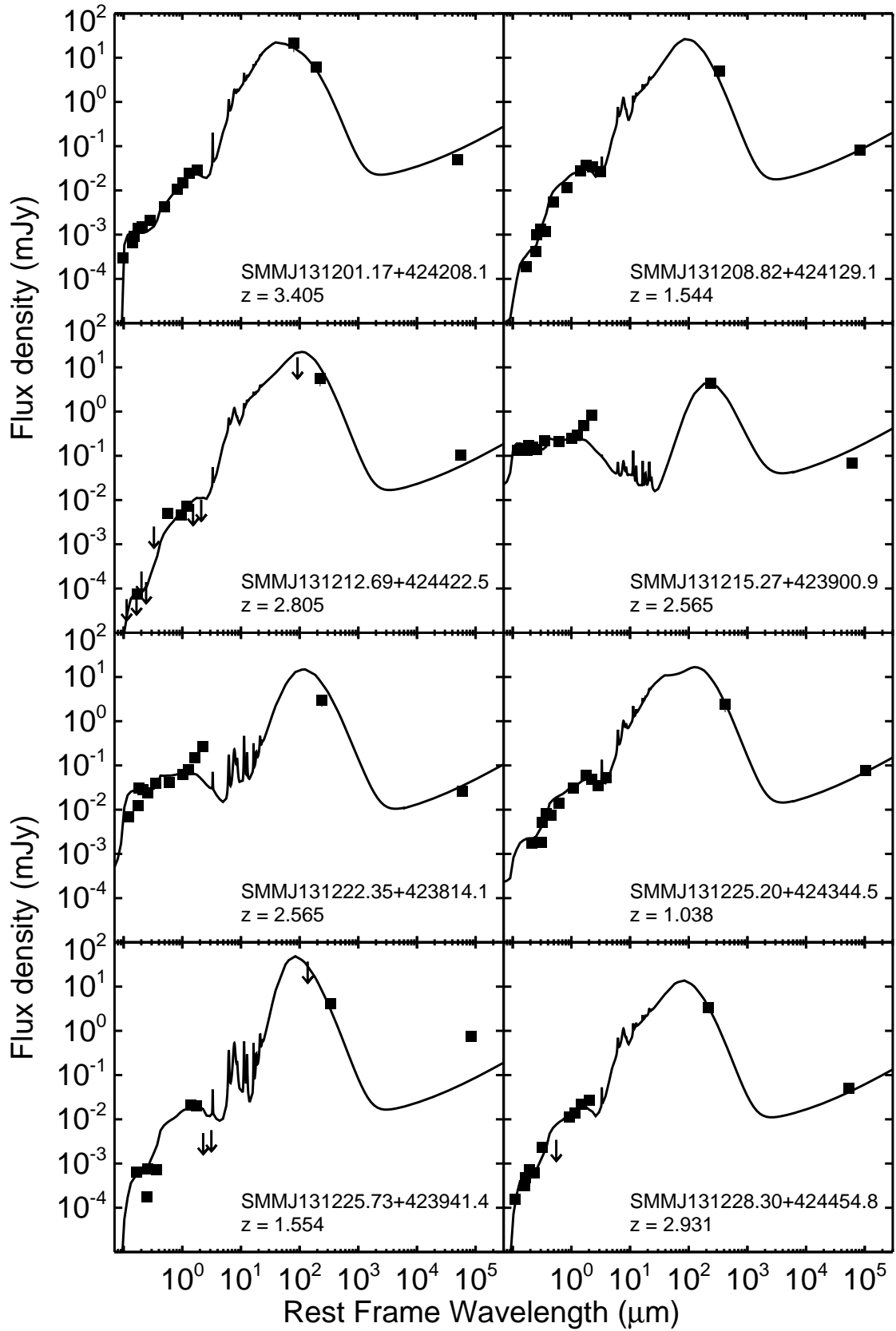


Fig. A.1 (continued).

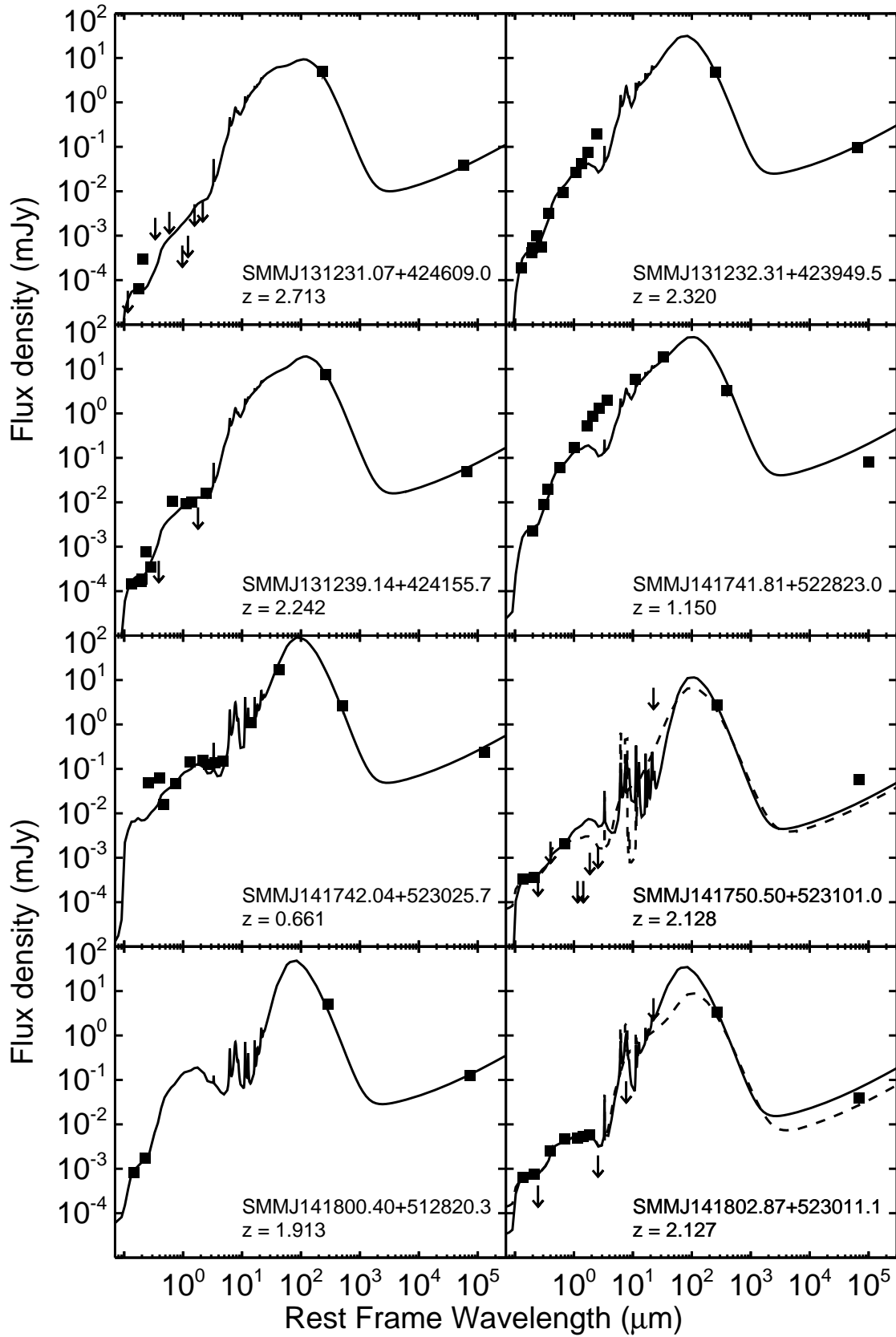


Fig. A.1 (continued).

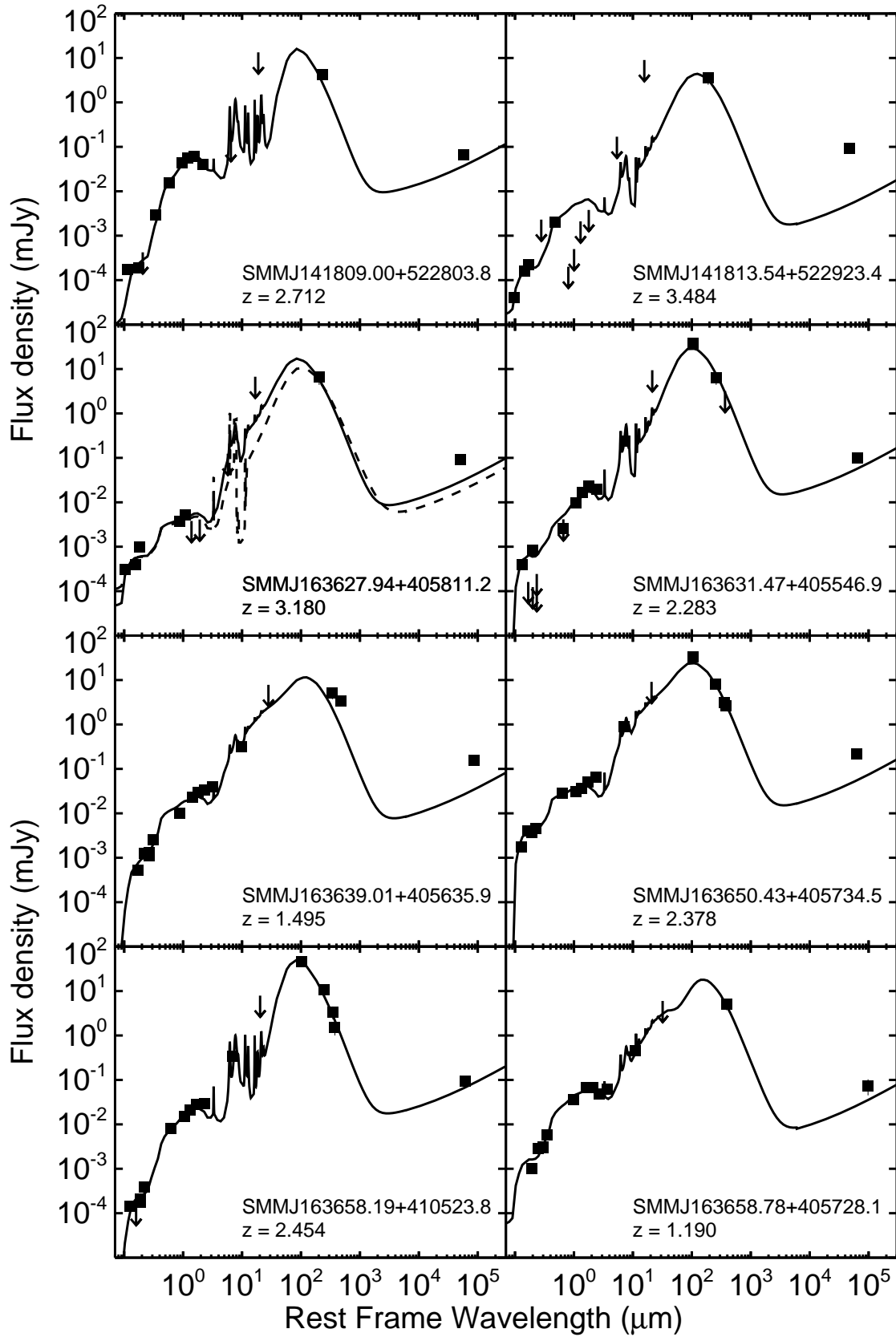


Fig. A.1 (continued).

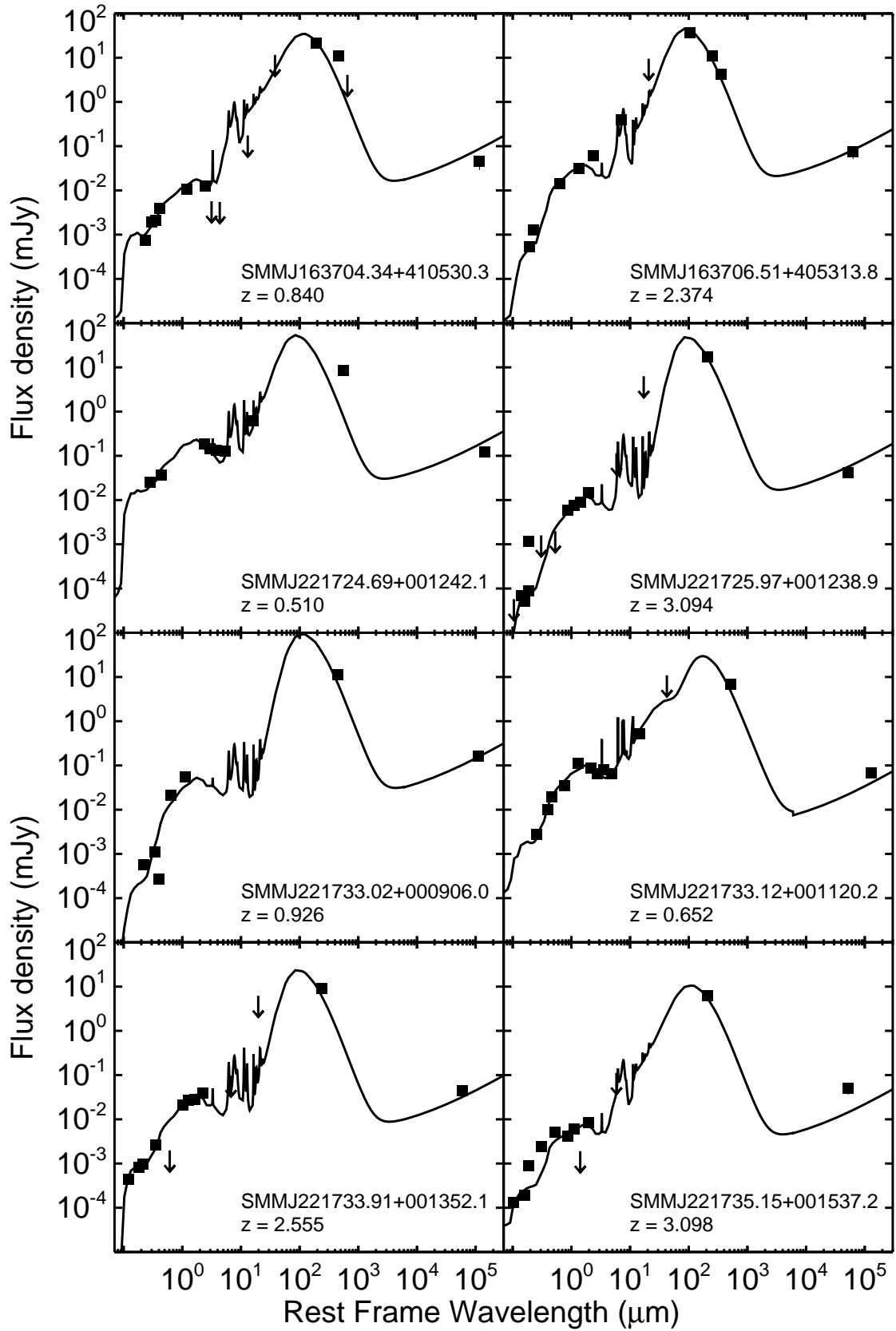


Fig. A.1 (continued).

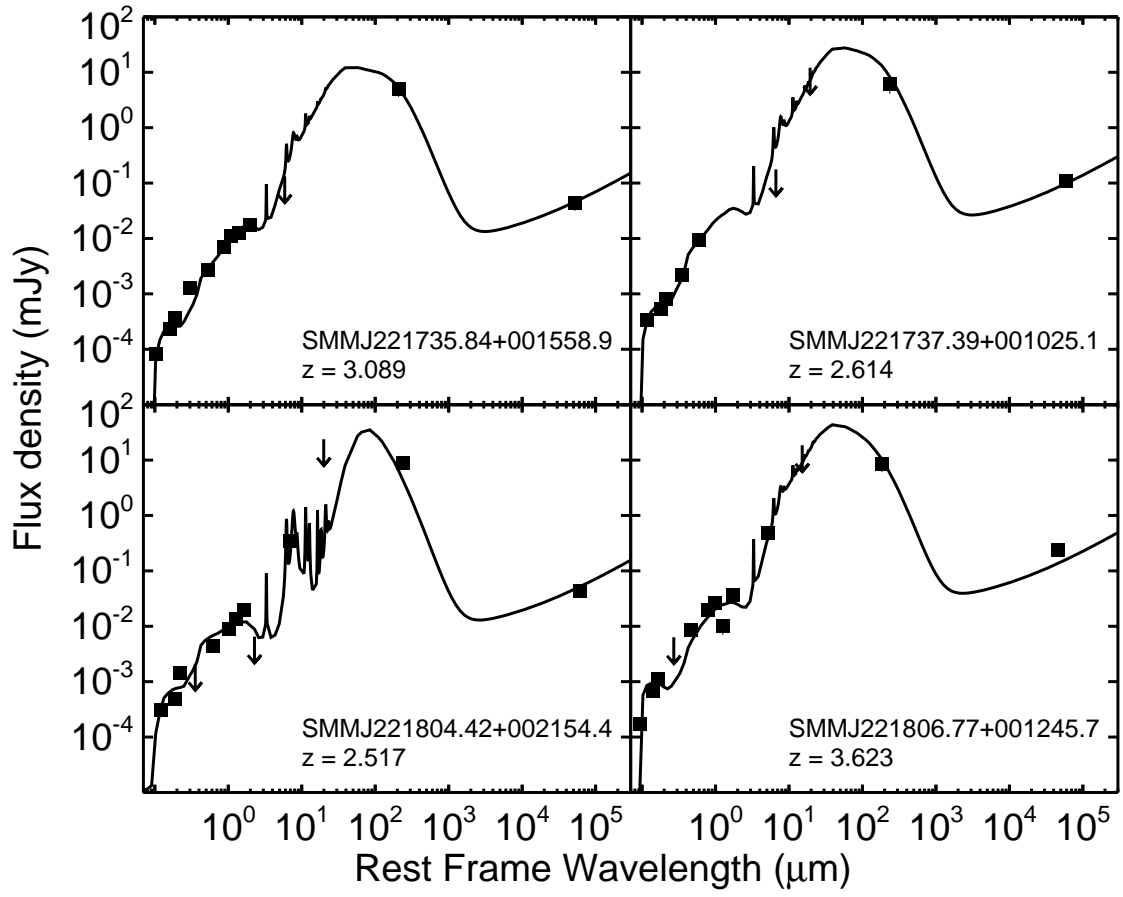


Fig. A.1 (continued).

Table A.4. Compilation of star formation rate density determinations in $M_{\odot} \text{ yr}^{-1} \text{ Mpc}^{-3}$

z	Δz	ρ_{SFR}	$-\Delta\rho_{\text{SFR}}$	$+\Delta\rho_{\text{SFR}}$	Estimator	Reference
3.780	0.340	0.1690	0.0218	0.0250	UV	Giavalisco et al. (2004); Hopkins (2004)
4.920	0.330	0.1089	0.0300	0.0414	UV	Giavalisco et al. (2004); Hopkins (2004)
5.740	0.360	0.1194	0.0423	0.0655	UV	Giavalisco et al. (2004); Hopkins (2004)
0.350	0.150	0.0356	0.0058	0.0070	UV	Wilson et al. (2002); Hopkins (2004)
0.800	0.200	0.0656	0.0110	0.0133	UV	Wilson et al. (2002); Hopkins (2004)
1.350	0.250	0.0925	0.0259	0.0361	UV	Wilson et al. (2002); Hopkins (2004)
1.500	0.500	0.1954	0.0721	0.1143	UV	Massarotti et al. (2001); Hopkins (2004)
2.750	0.750	0.3076	0.1135	0.1799	UV	Massarotti et al. (2001); Hopkins (2004)
4.000	0.500	0.1300	0.0569	0.1012	UV	Massarotti et al. (2001); Hopkins (2004)
0.150	0.150	0.0395	0.0043	0.0048	UV	Sullivan et al. (2000); Hopkins (2004)
3.040	0.250	0.1603	0.0174	0.0196	UV	Steidel et al. (1999); Hopkins (2004)
4.130	0.300	0.1245	0.0256	0.0322	UV	Steidel et al. (1999); Hopkins (2004)
0.700	0.200	0.0481	0.0102	0.0130	UV	Cowie et al. (1999); Hopkins (2004)
1.250	0.250	0.0652	0.0154	0.0201	UV	Cowie et al. (1999); Hopkins (2004)
0.150	0.150	0.0428	0.0125	0.0176	UV	Treyer et al. (1998); Hopkins (2004)
0.750	0.250	0.1019	0.0297	0.0420	UV	Connolly et al. (1997); Hopkins (2004)
1.250	0.250	0.1368	0.0399	0.0564	UV	Connolly et al. (1997); Hopkins (2004)
1.750	0.250	0.1062	0.0310	0.0438	UV	Connolly et al. (1997); Hopkins (2004)
0.350	0.150	0.0289	0.0043	0.0051	UV	Lilly et al. (1996); Hopkins (2004)
0.625	0.125	0.0542	0.0091	0.0110	UV	Lilly et al. (1996); Hopkins (2004)
0.875	0.125	0.1050	0.0307	0.0433	UV	Lilly et al. (1996); Hopkins (2004)
4.850	0.450	0.0350	0.0150	0.0150	UV	Iwata et al. (2003); van Breukelen et al. (2005)
0.700	0.300	0.0462	0.0060	0.0068	UV	Cowie et al. (1996); Somerville et al. (2001)
1.250	0.250	0.0668	0.0195	0.0276	UV	Cowie et al. (1996); Somerville et al. (2001)
0.350	0.150	0.0495	0.0258	0.0272	UV	Sawicki et al. (1997); Somerville et al. (2001)
0.750	0.250	0.0733	0.0109	0.0089	UV	Sawicki et al. (1997); Somerville et al. (2001)
1.500	0.500	0.0988	0.0087	0.0095	UV	Sawicki et al. (1997); Somerville et al. (2001)
2.500	0.500	0.2113	0.0273	0.0313	UV	Sawicki et al. (1997); Somerville et al. (2001)
3.500	0.500	0.0922	0.0190	0.0187	UV	Sawicki et al. (1997); Somerville et al. (2001)
0.250	0.250	0.0569	0.0226	0.0592	UV	Pascarelle et al. (1998); Somerville et al. (2001)
0.750	0.250	0.0638	0.0176	0.0446	UV	Pascarelle et al. (1998); Somerville et al. (2001)
1.250	0.250	0.0901	0.0218	0.0665	UV	Pascarelle et al. (1998); Somerville et al. (2001)
1.750	0.250	0.0922	0.0223	0.0681	UV	Pascarelle et al. (1998); Somerville et al. (2001)
2.500	0.500	0.0556	0.0213	0.0503	UV	Pascarelle et al. (1998); Somerville et al. (2001)
3.500	0.500	0.0519	0.0240	0.0616	UV	Pascarelle et al. (1998); Somerville et al. (2001)
4.500	0.500	0.0653	0.0374	0.1145	UV	Pascarelle et al. (1998); Somerville et al. (2001)
5.500	0.500	0.0285	0.0166	0.0824	UV	Pascarelle et al. (1998); Somerville et al. (2001)
0.315	0.115	0.0373	0.0005	0.0005	UV	Mobasher et al. (2009)
0.540	0.110	0.0533	0.0005	0.0006	UV	Mobasher et al. (2009)
0.765	0.115	0.0957	0.0006	0.0006	UV	Mobasher et al. (2009)
0.990	0.110	0.1082	0.0006	0.0006	UV	Mobasher et al. (2009)
3.800	0.350	0.0891	0.0097	0.0109	UV	Bouwens et al. (2007)
5.000	0.350	0.0331	0.0043	0.0049	UV	Bouwens et al. (2007)
5.900	0.300	0.0224	0.0038	0.0045	UV	Bouwens et al. (2007)
4.000	0.500	0.0362	0.0050	0.0050	UV	Ouchi et al. (2004)
4.700	0.500	0.0300	0.0175	0.0175	UV	Ouchi et al. (2004)
4.900	0.300	0.0138	0.0069	0.0069	UV	Ouchi et al. (2004)
4.000	0.500	0.0300	0.0025	0.0025	UV	Ouchi et al. (2004)
4.700	0.500	0.0200	0.0088	0.0088	UV	Ouchi et al. (2004)
4.900	0.300	0.0088	0.0044	0.0044	UV	Ouchi et al. (2004)
5.850	0.250	0.0034	0.0014	0.0014	UV	Stanway et al. (2003)
1.000	0.500	0.2080	0.0990	0.0990	UV	Thompson et al. (2006)
2.000	0.500	0.3980	0.1800	0.1800	UV	Thompson et al. (2006)
3.000	0.500	0.3220	0.1600	0.1600	UV	Thompson et al. (2006)
4.000	0.500	0.0940	0.0390	0.0390	UV	Thompson et al. (2006)
5.000	0.500	0.0410	0.0160	0.0160	UV	Thompson et al. (2006)
6.000	0.500	0.1260	0.0740	0.0740	UV	Thompson et al. (2006)
2.280	0.330	0.1778	0.1407	0.6733	UV	Ly et al. (2009)
4.000	0.300	0.1301	0.0194	0.0227	UV	Yoshida et al. (2006); Ly et al. (2009)
4.700	0.300	0.0745	0.0316	0.0550	UV	Yoshida et al. (2006); Ly et al. (2009)

Table A.4. continued.

z	Δz	ρ_{SFR}	$-\Delta\rho_{\text{SFR}}$	$+\Delta\rho_{\text{SFR}}$	Estimator	Reference
2.300	0.400	0.1500	0.0223	0.0262	UV	Reddy et al. (2008); Ly et al. (2009)
0.050	0.050	0.0126	0.0026	0.0033	UV	Wyder et al. (2005)
3.200	0.140	0.1600	0.0798	0.1592	UV	Shim et al. (2007)
0.330	0.040	0.0353	0.0059	0.0071	UV	Dahlen et al. (2007)
0.545	0.085	0.0996	0.0148	0.0174	UV	Dahlen et al. (2007)
1.125	0.205	0.1283	0.0240	0.0295	UV	Dahlen et al. (2007)
1.750	0.130	0.1898	0.0390	0.0491	UV	Dahlen et al. (2007)
2.225	0.145	0.1407	0.0364	0.0491	UV	Dahlen et al. (2007)
2.750	0.750	0.1800	0.0337	0.0414	UV	Wadadekar et al. (2006)
0.900	0.500	0.0989	0.0221	0.0285	[O 2]	Teplitz et al. (2003); Hopkins (2004)
0.025	0.025	0.0122	0.0036	0.0050	[O 2]	Gallego et al. (2002); Hopkins (2004)
0.200	0.100	0.0136	0.0032	0.0062	[O 2]	Hogg et al. (1998); Hopkins (2004)
0.300	0.100	0.0119	0.0023	0.0031	[O 2]	Hogg et al. (1998); Hopkins (2004)
0.400	0.100	0.0536	0.0095	0.0147	[O 2]	Hogg et al. (1998); Hopkins (2004)
0.500	0.100	0.0955	0.0137	0.0180	[O 2]	Hogg et al. (1998); Hopkins (2004)
0.600	0.100	0.0649	0.0086	0.0117	[O 2]	Hogg et al. (1998); Hopkins (2004)
0.700	0.100	0.0535	0.0083	0.0120	[O 2]	Hogg et al. (1998); Hopkins (2004)
0.800	0.100	0.0566	0.0085	0.0116	[O 2]	Hogg et al. (1998); Hopkins (2004)
0.900	0.100	0.0714	0.0112	0.0165	[O 2]	Hogg et al. (1998); Hopkins (2004)
1.000	0.100	0.1146	0.0208	0.0320	[O 2]	Hogg et al. (1998); Hopkins (2004)
1.100	0.100	0.0899	0.0242	0.0523	[O 2]	Hogg et al. (1998); Hopkins (2004)
1.200	0.100	0.0859	0.0286	0.0859	[O 2]	Hogg et al. (1998); Hopkins (2004)
0.375	0.125	0.0197	0.0033	0.0034	[O 2]	Hammer et al. (1997); Hopkins (2004)
0.625	0.125	0.0594	0.0174	0.0171	[O 2]	Hammer et al. (1997); Hopkins (2004)
0.875	0.125	0.1396	0.0814	0.0817	[O 2]	Hammer et al. (1997); Hopkins (2004)
0.401	0.011	0.0240	0.0080	0.0080	[O 3]	Hippelein et al. (2003)
0.636	0.010	0.0720	0.0160	0.0160	[O 3]	Hippelein et al. (2003)
0.881	0.014	0.1070	0.0350	0.0350	[O 2]	Hippelein et al. (2003)
1.193	0.018	0.2280	0.0550	0.0550	[O 2]	Hippelein et al. (2003)
2.750	0.750	0.2773	0.0810	0.1144	H β	Pettini et al. (1998); Hopkins (2004)
0.025	0.025	0.0249	0.0056	0.0072	H α	Pérez-González et al. (2003); Hopkins (2004)
0.800	0.300	0.1172	0.0262	0.0338	H α	Tresse et al. (2002); Hopkins (2004)
2.200	0.050	0.2655	0.0641	0.0845	H α	Moorwood et al. (2000); Hopkins (2004)
1.250	0.550	0.2350	0.0137	0.0145	H α	Hopkins et al. (2000); Hopkins (2004)
0.150	0.150	0.0151	0.0020	0.0022	H α	Sullivan et al. (2000); Hopkins (2004)
0.900	0.100	0.1067	0.0294	0.0440	H α	Glazebrook et al. (1999); Hopkins (2004)
1.300	0.600	0.2799	0.0676	0.0891	H α	Yan et al. (1999); Hopkins (2004)
0.200	0.100	0.0324	0.0042	0.0048	H α	Tresse & Maddox (1998); Hopkins (2004)
0.022	0.022	0.0126	0.0046	0.0074	H α	Gallego et al. (1995); Hopkins (2004)
0.043	0.043	0.0240	0.0026	0.0029	H α	Gronwall (1999); Somerville et al. (2001)
0.243	0.009	0.0360	0.0120	0.0060	H α	Fujita et al. (2003b)
0.245	0.007	0.0240	0.0060	0.0060	H α	Hippelein et al. (2003)
0.100	0.100	0.0192	0.0042	0.0014	H α	Brinchmann et al. (2004)
0.010	0.010	0.0158	0.0033	0.0071	H α	Hanish et al. (2006)
0.840	0.030	0.1500	0.0200	0.0200	H α	Sobral et al. (2009)
2.230	0.150	0.1700	0.0900	0.1600	H α	Geach et al. (2008)
0.242	0.009	0.0180	0.0040	0.0070	H α	Shioya et al. (2008)
0.840	0.030	0.1700	0.0300	0.0300	H α	Villar et al. (2008)
2.300	0.400	0.3484	0.0869	0.0869	H α	Reddy et al. (2008)
3.050	0.350	0.2141	0.0450	0.0450	H α	Reddy et al. (2008)
0.350	0.150	0.0365	0.0169	0.0314	mid-IR	Flores et al. (1999); Hopkins (2004)
0.625	0.125	0.0678	0.0297	0.0527	mid-IR	Flores et al. (1999); Hopkins (2004)
0.875	0.125	0.1337	0.0602	0.1096	mid-IR	Flores et al. (1999); Hopkins (2004)
0.215	0.215	0.0300	0.0100	0.0200	mid-IR	Mann et al. (2002)
0.515	0.085	0.0700	0.0100	0.0200	mid-IR	Mann et al. (2002)
0.100	0.100	0.0175	0.0049	0.0049	mid-IR	Pozzi et al. (2004)
0.300	0.100	0.0301	0.0140	0.0140	mid-IR	Pozzi et al. (2004)
0.300	0.100	0.0197	0.0067	0.0066	mid-IR	Zheng et al. (2007)
0.500	0.100	0.0349	0.0088	0.0088	mid-IR	Zheng et al. (2007)
0.700	0.100	0.0570	0.0096	0.0101	mid-IR	Zheng et al. (2007)
0.900	0.100	0.0616	0.0120	0.0121	mid-IR	Zheng et al. (2007)

Table A.4. continued.

z	Δz	ρ_{SFR}	$-\Delta\rho_{\text{SFR}}$	$+\Delta\rho_{\text{SFR}}$	Estimator	Reference
2.300	0.400	0.2091	0.0357	0.0357	mid-IR	Reddy et al. (2008)
3.050	0.350	0.1124	0.0211	0.0211	mid-IR	Reddy et al. (2008)
1.000	0.100	0.2000	0.0300	0.0300	mid-IR	Caputi et al. (2007)
2.000	0.300	0.1100	0.0200	0.0200	mid-IR	Caputi et al. (2007)
0.450	0.150	0.2750	0.0220	0.0220	mid-IR	Santini et al. (2009)
0.800	0.200	0.4870	0.0170	0.0170	mid-IR	Santini et al. (2009)
1.250	0.250	0.7550	0.0290	0.0290	mid-IR	Santini et al. (2009)
2.000	0.500	1.6590	0.0580	0.0580	mid-IR	Santini et al. (2009)
0.100	0.100	0.0180	0.0025	0.0029	mid-IR	Pérez-González et al. (2005)
0.100	0.100	0.0163	0.0023	0.0027	mid-IR	Pérez-González et al. (2005)
0.100	0.100	0.0171	0.0024	0.0028	mid-IR	Pérez-González et al. (2005)
0.300	0.100	0.0384	0.0019	0.0020	mid-IR	Pérez-González et al. (2005)
0.300	0.100	0.0356	0.0017	0.0018	mid-IR	Pérez-González et al. (2005)
0.300	0.100	0.0330	0.0016	0.0017	mid-IR	Pérez-González et al. (2005)
0.500	0.100	0.0818	0.0060	0.0064	mid-IR	Pérez-González et al. (2005)
0.500	0.100	0.0927	0.0089	0.0098	mid-IR	Pérez-González et al. (2005)
0.500	0.100	0.0589	0.0043	0.0046	mid-IR	Pérez-González et al. (2005)
0.700	0.100	0.1052	0.0052	0.0054	mid-IR	Pérez-González et al. (2005)
0.700	0.100	0.1459	0.0140	0.0155	mid-IR	Pérez-González et al. (2005)
0.700	0.100	0.0951	0.0047	0.0049	mid-IR	Pérez-González et al. (2005)
0.900	0.100	0.1319	0.0580	0.1036	mid-IR	Pérez-González et al. (2005)
0.900	0.100	0.1877	0.0852	0.1559	mid-IR	Pérez-González et al. (2005)
0.900	0.100	0.1255	0.0552	0.0985	mid-IR	Pérez-González et al. (2005)
1.200	0.200	0.1741	0.0127	0.0137	mid-IR	Pérez-González et al. (2005)
1.200	0.200	0.2477	0.0400	0.0478	mid-IR	Pérez-González et al. (2005)
1.200	0.200	0.1423	0.0136	0.0151	mid-IR	Pérez-González et al. (2005)
1.600	0.200	0.1574	0.0151	0.0167	mid-IR	Pérez-González et al. (2005)
1.600	0.200	0.2076	0.0379	0.0464	mid-IR	Pérez-González et al. (2005)
1.600	0.200	0.1353	0.0130	0.0143	mid-IR	Pérez-González et al. (2005)
2.000	0.200	0.1319	0.0344	0.0466	mid-IR	Pérez-González et al. (2005)
2.000	0.200	0.2239	0.0705	0.1028	mid-IR	Pérez-González et al. (2005)
2.000	0.200	0.1388	0.0362	0.0490	mid-IR	Pérez-González et al. (2005)
2.400	0.200	0.1785	0.0432	0.0570	mid-IR	Pérez-González et al. (2005)
2.400	0.200	0.3524	0.1109	0.1618	mid-IR	Pérez-González et al. (2005)
2.400	0.200	0.2296	0.0556	0.0733	mid-IR	Pérez-González et al. (2005)
0.698	0.618	0.0102	0.0014	0.0014	submm	This work
1.775	0.367	0.0228	0.0027	0.0027	submm	This work
2.357	0.209	0.0486	0.0054	0.0054	submm	This work
3.101	0.522	0.0341	0.0040	0.0040	submm	This work
2.000	1.000	0.1476	0.0607	0.0973	submm	Barger et al. (2000); Hopkins (2004)
4.500	1.500	0.1901	0.1195	0.2454	submm	Barger et al. (2000); Hopkins (2004)
0.057	0.041	0.0206	0.0016	0.0024	submm	Pascale et al. (2009)
0.138	0.040	0.0292	0.0022	0.0040	submm	Pascale et al. (2009)
0.250	0.073	0.0192	0.0026	0.0036	submm	Pascale et al. (2009)
0.454	0.132	0.0511	0.0022	0.0067	submm	Pascale et al. (2009)
0.824	0.239	0.0785	0.0073	0.0086	submm	Pascale et al. (2009)
2.281	1.219	0.1104	0.0092	0.0140	submm	Pascale et al. (2009)
0.005	0.005	0.0109	0.0007	0.0008	radio	Condon et al. (2002); Hopkins (2004)
0.080	0.080	0.0187	0.0035	0.0038	radio	Sadler et al. (2002); Hopkins (2004)
0.010	0.010	0.0177	0.0036	0.0036	radio	Serjeant et al. (2002); Hopkins (2004)
0.070	0.070	0.0120	0.0025	0.0031	radio	Machalski & Godłowski (2000); Hopkins (2004)
0.206	0.196	0.0408	0.0157	0.0155	radio	Haarsma et al. (2000); Hopkins (2004)
0.464	0.054	0.0667	0.0246	0.0254	radio	Haarsma et al. (2000); Hopkins (2004)
0.623	0.075	0.0764	0.0344	0.0340	radio	Haarsma et al. (2000); Hopkins (2004)
0.804	0.080	0.1315	0.0446	0.0459	radio	Haarsma et al. (2000); Hopkins (2004)
1.600	0.640	0.1641	0.0557	0.0522	radio	Haarsma et al. (2000); Hopkins (2004)
0.005	0.005	0.0209	0.0000	0.0000	radio	Condon (1989); Hopkins (2004)
0.152	0.149	0.0220	0.0010	0.0010	radio	Mauch & Sadler (2007)
0.310	0.210	0.0331	0.0074	0.0076	radio	Seymour et al. (2008)
0.810	0.290	0.0851	0.0262	0.0271	radio	Seymour et al. (2008)
1.500	0.400	0.1479	0.0666	0.0812	radio	Seymour et al. (2008)

Table A.4. continued.

z	Δz	ρ_{SFR}	$-\Delta\rho_{\text{SFR}}$	$+\Delta\rho_{\text{SFR}}$	Estimator	Reference
2.450	0.550	0.1202	0.0756	0.1036	radio	Seymour et al. (2008)
0.100	0.100	0.0087	0.0063	0.0062	radio	Dunne et al. (2009)
0.300	0.100	0.0292	0.0107	0.0106	radio	Dunne et al. (2009)
0.500	0.100	0.0385	0.0118	0.0106	radio	Dunne et al. (2009)
0.700	0.100	0.0700	0.0175	0.0164	radio	Dunne et al. (2009)
0.900	0.100	0.0781	0.0202	0.0172	radio	Dunne et al. (2009)
1.100	0.100	0.1124	0.0262	0.0249	radio	Dunne et al. (2009)
1.300	0.100	0.1327	0.0287	0.0257	radio	Dunne et al. (2009)
1.500	0.100	0.2043	0.0369	0.0343	radio	Dunne et al. (2009)
1.700	0.100	0.1788	0.0339	0.0277	radio	Dunne et al. (2009)
1.900	0.100	0.1582	0.0256	0.0245	radio	Dunne et al. (2009)
2.250	0.250	0.1061	0.0141	0.0125	radio	Dunne et al. (2009)
2.750	0.250	0.1049	0.0150	0.0123	radio	Dunne et al. (2009)
3.250	0.250	0.0583	0.0078	0.0069	radio	Dunne et al. (2009)
4.250	0.750	0.0184	0.0032	0.0026	radio	Dunne et al. (2009)
0.150	0.150	0.0383	0.0131	0.0251	X-ray	Georgakakis et al. (2003); Hopkins (2004)
2.750	0.750	>0.0607			UV	Madau et al. (1996); Hopkins (2004)
4.000	0.500	>0.0189			UV	Madau et al. (1996); Hopkins (2004)
2.750	0.750	>0.0290			UV	Madau et al. (1998); van Breukelen et al. (2005)
4.000	0.500	>0.0110			UV	Madau et al. (1998); van Breukelen et al. (2005)
3.200	0.140	>0.0033			UV	Shim et al. (2007)
2.200	0.350	>0.0372			UV	Sawicki & Thompson (2006a,b); Ly et al. (2009)
2.960	0.260	>0.0370			UV	Sawicki & Thompson (2006a,b); Ly et al. (2009)
4.130	0.260	>0.0161			UV	Sawicki & Thompson (2006a,b); Ly et al. (2009)
3.500	0.500	>0.0442			UV	Paltani et al. (2007); Ly et al. (2009)
2.700	0.700	>0.0282			UV	Bouwens et al. (2003a)
3.850	0.450	>0.0166			UV	Bouwens et al. (2003a)
4.700	0.200	>0.0147			UV	Bouwens et al. (2003a)
6.000	0.200	>0.0360			UV	Bouwens et al. (2003b)
5.900	0.200	>0.0070			UV	Bouwens et al. (2004)
5.900	0.200	>0.0073			UV	Bouwens et al. (2006)
5.900	0.200	>0.0221			UV	Bouwens et al. (2006)
6.000	0.400	>0.0050			UV	Bunker et al. (2004)
3.050	0.350	>0.0321			UV	Reddy et al. (2008)
5.000	0.500	>0.0137			UV	Iwata et al. (2007)
5.900	0.300	>0.0003			UV	Shimasaku et al. (2005)
5.850	0.250	>0.0034			UV	Stanway et al. (2003)
2.259	0.053	>0.0054			Ly α	Nilsson et al. (2009)
2.379	0.023	>0.0024			Ly α	Palunas et al. (2004)
3.110	0.020	>0.0120			Ly α	Gronwall et al. (2007)
3.156	0.025	>0.0130			Ly α	Nilsson et al. (2007)
3.135	0.045	>0.0043			Ly α	Ouchi et al. (2008)
3.140	0.040	>0.0300			Ly α	Kudritzki et al. (2000)
3.400	0.030	>0.0060			Ly α	Hu et al. (1998)
3.438	0.033	>0.0100			Ly α	Cowie & Hu (1998)
3.463	0.982	>0.0220			Ly α	van Breukelen et al. (2005)
3.690	0.060	>0.0021			Ly α	Ouchi et al. (2008)
3.700	0.220	>0.0004			Ly α	Fujita et al. (2003a); van Breukelen et al. (2005)
4.500	0.064	>0.0100			Ly α	Hu et al. (1998)
4.860	0.030	>0.0063			Ly α	Ouchi et al. (2003); van Breukelen et al. (2005)
5.690	0.090	>0.0032			Ly α	Ouchi et al. (2008)
5.700	0.100	>0.0012			Ly α	Ajiki et al. (2003)
5.700	0.050	>0.0018			Ly α	Malhotra & Rhoads (2004)
5.700	0.050	>0.0023			Ly α	Shimasaku et al. (2006)
5.700	0.050	>0.0007			Ly α	Murayama et al. (2007)
5.735	0.062	>0.0005			Ly α	Rhoads et al. (2003)
6.500	0.050	>0.0036			Ly α	Malhotra & Rhoads (2004)
6.550	0.050	>0.0006			Ly α	Taniguchi et al. (2005)
6.578	0.002	>0.0005			Ly α	Kodaira et al. (2003)
3.000	1.000	>0.0818			submm	Hughes et al. (1998); Hopkins (2004)

Note. — Lower limits indicate value not corrected for extinction. The data with double reference were taken directly from the compilation given in the second reference. This table is available in a machine-readable form in the electronic edition of the Journal.

Table A.5. Compilation of stellar mass density determinations in $\log M_{\odot} \text{Mpc}^{-3}$

z	Δz	ρ_*	$-\Delta\rho_*$	$+\Delta\rho_*$	Reference
0.698	0.618	7.12	0.08	0.13	This work
1.775	0.367	7.18	0.11	0.16	This work
2.357	0.209	7.61	0.08	0.12	This work
3.101	0.522	7.28	0.07	0.12	This work
0.100	0.100	8.48	0.10	0.10	Borch et al. (2006)
0.300	0.100	8.34	0.15	0.15	Borch et al. (2006)
0.500	0.100	8.32	0.11	0.11	Borch et al. (2006)
0.700	0.100	8.33	0.10	0.10	Borch et al. (2006)
0.900	0.100	8.17	0.18	0.18	Borch et al. (2006)
0.100	0.100	8.49	0.05	0.04	Rudnick et al. (2003)
1.120	0.480	8.14	0.10	0.11	Rudnick et al. (2003)
2.010	0.400	7.48	0.16	0.12	Rudnick et al. (2003)
2.800	0.400	7.49	0.14	0.12	Rudnick et al. (2003)
0.950	0.450	8.46	0.07	0.07	Dickinson et al. (2003)
1.700	0.300	8.06	0.13	0.17	Dickinson et al. (2003)
2.250	0.250	7.58	0.07	0.11	Dickinson et al. (2003)
2.750	0.250	7.52	0.14	0.23	Dickinson et al. (2003)
0.950	0.450	8.61	0.07	0.07	Dickinson et al. (2003)
1.700	0.300	8.22	0.12	0.16	Dickinson et al. (2003)
2.250	0.250	8.01	0.08	0.09	Dickinson et al. (2003)
2.750	0.250	7.89	0.15	0.20	Dickinson et al. (2003)
0.950	0.450	8.52	0.08	0.07	Dickinson et al. (2003)
1.700	0.300	7.97	0.17	0.17	Dickinson et al. (2003)
2.250	0.250	7.36	0.08	0.11	Dickinson et al. (2003)
2.750	0.250	7.27	0.18	0.27	Dickinson et al. (2003)
0.375	0.125	8.65	0.17	0.12	Cohen (2002)
0.650	0.150	8.65	0.01	0.08	Cohen (2002)
0.925	0.125	8.62	0.09	0.08	Cohen (2002)
0.500	0.100	8.83	0.04	0.04	Drory et al. (2004, 2005)
0.700	0.100	8.76	0.04	0.04	Drory et al. (2004, 2005)
0.900	0.100	8.60	0.04	0.04	Drory et al. (2004, 2005)
1.100	0.100	8.55	0.04	0.04	Drory et al. (2004, 2005)
0.500	0.250	8.50	0.27	0.27	Drory et al. (2004, 2005)
0.500	0.250	8.51	0.17	0.17	Drory et al. (2004, 2005)
1.000	0.250	8.42	0.12	0.12	Drory et al. (2004, 2005)
1.000	0.250	8.29	0.19	0.19	Drory et al. (2004, 2005)
1.500	0.250	8.38	0.16	0.16	Drory et al. (2004, 2005)
1.500	0.250	8.03	0.16	0.16	Drory et al. (2004, 2005)
2.000	0.250	8.09	0.19	0.19	Drory et al. (2004, 2005)
2.000	0.250	8.04	0.20	0.20	Drory et al. (2004, 2005)
2.625	0.375	8.15	0.19	0.19	Drory et al. (2004, 2005)
2.625	0.375	7.78	0.20	0.20	Drory et al. (2004, 2005)
3.500	0.500	7.92	0.17	0.17	Drory et al. (2004, 2005)
3.500	0.500	7.68	0.20	0.20	Drory et al. (2004, 2005)
4.500	0.500	7.37	0.26	0.26	Drory et al. (2004, 2005)
4.500	0.500	7.43	0.20	0.20	Drory et al. (2004, 2005)
0.900	0.100	8.18	0.13	0.10	Glazebrook et al. (2004)
1.200	0.100	7.82	0.13	0.01	Glazebrook et al. (2004)
1.450	0.150	8.08	0.09	0.08	Glazebrook et al. (2004)
1.800	0.200	7.69	0.13	0.11	Glazebrook et al. (2004)
0.500	0.100	8.32	0.03	0.03	Fontana et al. (2003, 2004, 2006)
0.700	0.100	8.53	0.02	0.02	Fontana et al. (2003, 2004, 2006)
0.900	0.100	8.16	0.03	0.03	Fontana et al. (2003, 2004, 2006)
1.150	0.150	8.26	0.02	0.02	Fontana et al. (2003, 2004, 2006)
1.450	0.150	7.96	0.03	0.03	Fontana et al. (2003, 2004, 2006)
1.800	0.200	7.90	0.04	0.04	Fontana et al. (2003, 2004, 2006)
2.500	0.500	7.60	0.04	0.04	Fontana et al. (2003, 2004, 2006)
3.500	0.500	7.23	0.12	0.12	Fontana et al. (2003, 2004, 2006)
4.500	0.500	7.73	0.12	0.12	Fontana et al. (2003, 2004, 2006)
5.500	0.500	7.84	0.12	0.12	Fontana et al. (2003, 2004, 2006)

Table A.5. continued.

z	Δz	ρ_*	$-\Delta\rho_*$	$+\Delta\rho_*$	Reference
0.450	0.250	8.51	0.04	0.24	Fontana et al. (2003, 2004, 2006)
0.850	0.150	8.44	0.05	0.20	Fontana et al. (2003, 2004, 2006)
1.250	0.250	8.19	0.11	0.13	Fontana et al. (2003, 2004, 2006)
1.750	0.250	7.86	0.24	0.24	Fontana et al. (2003, 2004, 2006)
2.250	0.250	7.65	0.24	0.24	Fontana et al. (2003, 2004, 2006)
0.500	0.250	8.64	0.17	0.24	Fontana et al. (2003, 2004, 2006)
1.000	0.250	8.29	0.31	0.35	Fontana et al. (2003, 2004, 2006)
1.625	0.375	7.87	0.28	0.35	Fontana et al. (2003, 2004, 2006)
2.250	0.250	7.92	0.42	0.26	Fontana et al. (2003, 2004, 2006)
2.850	0.350	7.90	0.20	0.38	Fontana et al. (2003, 2004, 2006)
0.100	0.100	8.75	0.07	0.06	Cole et al. (2001)
0.350	0.150	8.53	0.13	0.09	Brinchmann & Ellis (2000)
0.625	0.125	8.56	0.05	0.06	Brinchmann & Ellis (2000)
0.875	0.125	8.48	0.04	0.06	Brinchmann & Ellis (2000)
0.100	0.100	8.75	0.12	0.12	Pérez-González et al. (2008)
0.300	0.100	8.61	0.06	0.06	Pérez-González et al. (2008)
0.500	0.100	8.57	0.04	0.04	Pérez-González et al. (2008)
0.700	0.100	8.52	0.05	0.05	Pérez-González et al. (2008)
0.900	0.100	8.44	0.05	0.05	Pérez-González et al. (2008)
1.150	0.150	8.35	0.05	0.05	Pérez-González et al. (2008)
1.450	0.150	8.18	0.07	0.07	Pérez-González et al. (2008)
1.800	0.200	8.02	0.07	0.07	Pérez-González et al. (2008)
2.250	0.250	7.87	0.09	0.09	Pérez-González et al. (2008)
2.750	0.250	7.76	0.18	0.18	Pérez-González et al. (2008)
3.250	0.250	7.63	0.14	0.14	Pérez-González et al. (2008)
3.750	0.250	7.49	0.13	0.13	Pérez-González et al. (2008)
0.150	0.150	8.76	0.13	0.11	Salucci & Persic (1999)
0.097	0.084	8.73	0.07	0.06	Driver et al. (2007)
0.150	0.150	8.72	0.01	0.01	Bell et al. (2003)
0.950	0.450	8.45	0.07	0.06	Conselice et al. (2005)
1.700	0.300	7.74	0.22	0.15	Conselice et al. (2005)
2.250	0.250	7.36	0.40	0.21	Conselice et al. (2005)
2.750	0.250	7.30	0.92	0.27	Conselice et al. (2005)
0.500	0.250	8.57	0.03	0.03	Elsner et al. (2008)
1.000	0.250	8.37	0.02	0.02	Elsner et al. (2008)
1.500	0.250	8.22	0.03	0.03	Elsner et al. (2008)
2.000	0.250	8.10	0.04	0.04	Elsner et al. (2008)
2.500	0.250	7.93	0.04	0.04	Elsner et al. (2008)
3.500	0.500	7.59	0.05	0.05	Elsner et al. (2008)
4.500	0.500	6.90	0.08	0.08	Elsner et al. (2008)
3.960	0.290	7.01	0.06	0.05	Stark et al. (2009)
4.790	0.250	6.63	0.07	0.06	Stark et al. (2009)
6.010	0.250	6.29	0.09	0.07	Stark et al. (2009)
5.000	0.600	6.78	0.08	0.22	Stark et al. (2007)
6.000	0.300	6.40	0.00	0.51	Eyles et al. (2007)
6.000	0.500	6.59	0.55	0.24	Yan et al. (2006)
0.100	0.100	8.59	0.04	0.04	Rudnick et al. (2006)
0.500	0.500	8.05	0.03	0.07	Rudnick et al. (2006)
1.300	0.300	7.87	0.04	0.07	Rudnick et al. (2006)
2.000	0.400	7.76	0.06	0.06	Rudnick et al. (2006)
2.800	0.400	7.59	0.11	0.06	Rudnick et al. (2006)
0.100	0.100	8.51	0.07	0.07	Marchesini et al. (2009)
1.650	0.350	7.91	0.15	0.02	Marchesini et al. (2009)
2.500	0.500	7.55	0.18	0.12	Marchesini et al. (2009)
3.500	0.500	7.27	0.39	0.93	Marchesini et al. (2009)
0.550	0.150	8.31	0.07	0.07	Bundy et al. (2006)
0.875	0.125	8.30	0.10	0.10	Bundy et al. (2006)
1.200	0.200	8.15	0.10	0.10	Bundy et al. (2006)
0.300	0.100	8.46	0.03	0.03	Ilbert et al. (2010)
0.500	0.100	8.22	0.02	0.02	Ilbert et al. (2010)
0.700	0.100	8.25	0.02	0.02	Ilbert et al. (2010)

Table A.5. continued.

z	Δz	ρ_*	$-\Delta\rho_*$	$+\Delta\rho_*$	Reference
0.900	0.100	8.32	0.01	0.01	Ilbert et al. (2010)
1.100	0.100	8.09	0.02	0.02	Ilbert et al. (2010)
1.350	0.150	7.93	0.01	0.01	Ilbert et al. (2010)
1.750	0.250	7.72	0.09	0.14	Ilbert et al. (2010)
0.300	0.100	8.79	0.17	0.15	Arnouts et al. (2007)
0.500	0.100	8.63	0.11	0.12	Arnouts et al. (2007)
0.700	0.100	8.63	0.10	0.10	Arnouts et al. (2007)
0.900	0.100	8.73	0.13	0.13	Arnouts et al. (2007)
1.100	0.100	8.54	0.11	0.11	Arnouts et al. (2007)
1.350	0.150	8.43	0.12	0.12	Arnouts et al. (2007)
1.750	0.250	8.17	0.12	0.12	Arnouts et al. (2007)
0.325	0.225	8.66	0.10	0.10	Franceschini et al. (2006)
0.725	0.175	8.61	0.10	0.10	Franceschini et al. (2006)
1.150	0.250	8.45	0.10	0.10	Franceschini et al. (2006)
0.225	0.175	8.45	0.01	0.01	Pozzetti et al. (2007)
0.550	0.150	8.34	0.02	0.02	Pozzetti et al. (2007)
0.800	0.100	8.22	0.01	0.01	Pozzetti et al. (2007)
1.050	0.150	8.14	0.01	0.01	Pozzetti et al. (2007)
1.400	0.200	8.04	0.02	0.02	Pozzetti et al. (2007)
2.050	0.450	8.05	0.01	0.01	Pozzetti et al. (2007)
0.025	0.025	8.81	0.05	0.05	Kochanek et al. (2001)
0.100	0.100	8.72	0.03	0.03	Driver et al. (2006)
1.100	0.400	8.47	0.11	0.11	Gwyn & Hartwick (2005)
1.750	0.250	8.38	0.21	0.21	Gwyn & Hartwick (2005)
2.500	0.500	8.21	0.14	0.14	Gwyn & Hartwick (2005)
4.500	1.500	7.93	0.11	0.11	Gwyn & Hartwick (2005)
1.250	0.250	8.37	0.07	0.06	Caputi et al. (2006)
1.750	0.250	8.12	0.07	0.06	Caputi et al. (2006)

Note. — This table is available in a machine-readable form in the electronic edition of the Journal.